Characterizing Uncertainty to Manage Risk in Spacecraft Development with Application to Structures and Mass

by

Emily Baker Clements

Submitted to the Department of Aeronautics and Astronautics
in partial fulfillment of the requirements for the degree of

Master of Science in Aeronautics and Astronautics

at the

MASSACHUSETTS INSTITUTE OF TECHNOLOGY

June 2013

Author .....
Department of Aeronautics and Astronautics
May 23, 2013

Certified by .....
Kerri Cahoy
Assistant Professor
Thesis Supervisor

Accepted by .....
Eytan Modiano
Chairman, Department Committee on Graduate Theses

This work is sponsored by the Department of the Air Force under the United States Air Force contract number FA8721-05-C-0002. The opinions, interpretations, recommendations, and conclusions are those of the author and are not necessarily endorsed by the United States Government.

Characterizing Uncertainty to Manage Risk in Spacecraft Development with Application to Structures and Mass

by

Emily Baker Clements

Submitted to the Department of Aeronautics and Astronautics
on May 23, 2013, in partial fulfillment of the
requirements for the degree of
Master of Science in Aeronautics and Astronautics

Abstract

Most space programs experience significant cost and schedule growth over the course of program development. Poor uncertainty management has been identified as one of the leading causes of program cost and schedule overruns. Traditional methods of uncertainty management are deterministic, using industry standards to predict worst-case inputs and designing systems accordingly. However, this method can lead to inefficient use of resources due to excessive need for redesign of subsystems when other subsystems evolve. Improvements in computational power now allow more sophisticated uncertainty analysis methods using probabilistic techniques.

We propose a spacecraft design methodology that uses Monte Carlo and Gradient-based Sensitivity Analysis of system models to reduce program cost and schedule overruns by identifying design issues early when redesign is less expensive. We cover applications to mass budgets and finite element analysis to illustrate this methodology. The META complexity metric is a measure of uncertainty of a quantity of interest based on exponential entropy from information theory.

The Trapped Energetic Radiation Satellite (TERSat) structural design process is used as a test case to evaluate the methodology, with a focus on the mass budget and finite element analysis. While traditionally mass budget uncertainty is treated with margins and contingencies, we present a way to model the mass of a system and its components as probability distributions using studies of historical data to model the means and standard deviations. We propagate the uncertainties in the mass budget analysis through the TERSat finite element model to determine the effects of the uncertainty on structural analysis outputs. We show that uncertainty analysis and sensitivity analysis can help to identify design issues early and guide the redesign and refine processes for spacecraft development.

Thesis Supervisor: Kerri Cahoy
Title: Assistant Professor

Acknowledgments

This work was supported by the MIT Lincoln Laboratory Lincoln Scholars program.

I would like to thank my Lincoln Scholars mentor, Mark Padula, and my group leaders Dr. Jeff Mendenhall and Dr. Dennis Burianek for their support and advice. I would like to thank Professor David Miller for providing feedback on this research.

Throughout this research I had the opportunity to work with several people on the META program: Dr. Doug Allaire, Dr. Alessandra Babuscia, Professor John Deyst, Chelsea He, and Professor Karen Willcox. Their feedback on this research, particularly on statistics topics, made this research possible.

I would like to thank my advisor, Professor Kerri Cahoy. I have learned so much from her over the last two years.

I would like to thank my family for their love and support. Finally, I would like to thank my husband Austin for supporting me in all of my endeavors.

Contents

1 Introduction **17**

1.1 Motivations for Incorporating Space Program Uncertainty Statistics . 18

1.2 Research Objectives and Methodology 20

1.3 Literature Review 22

1.3.1 Measures of Complexity in Complex System Design and Implementation 22

1.3.2 Uncertainty of Quantities of Interest in Complex System Design and Implementation 25

1.3.3 Notes on Optimization 26

1.3.4 Current Practices in Complex Space System Uncertainty Management 27

1.4 TERSat Program Summary 28

2 Methodology **31**

2.1 Test System Setup 31

2.2 Test System: One Timestep Example 34

2.3 Test System: Continuing Timesteps Example 38

2.4 Test System: Parameter Variation 39

3 Overview of the TERSat Program **41**

3.1 Mission Overview 43

3.2 Requirements and Success Criteria 44

3.3 Design Overview 45

3.4 Technical Performance Measures 46
3.5 Payload Design 48
3.6 Program Schedule 50

4 Mass Budget Analysis **51**
4.1 Potential of Uncertainty Analysis to Reduce Cost and Schedule Growth 52
4.2 Traditional Approach 52
4.2.1 Literature on Space System Mass Budget Uncertainty 53
4.3 Methodology for Uncertainty Management in Mass Budgets 53
4.3.1 Shape of the Mass Probability Density Function 54
4.3.2 Monte Carlo Analysis 55
4.4 TERSat Mass Budget Case Study 55
4.4.1 Mass Budget Analysis of the Architecture Change Period Budget 55
4.4.2 Mass Budget Analysis with CDR Design Change 56
4.4.3 Results of Mass Budget Analysis 57
4.5 Mass Budget Analysis Conclusion 59

5 Finite Element Analysis **61**
5.1 Literature on Spacecraft Structure Uncertainty 62
5.2 TERSat Structural Design 63
5.3 Finite Element Analysis Baseline 63
5.3.1 Inputs 65
5.3.2 Assumptions 65
5.3.3 Model Approach 66
5.3.4 Baseline Analysis Results 68
5.3.5 Baseline Analysis Summary 74
5.4 Mass Budget Uncertainty Inputs 75
5.5 Monte Carlo Analysis of the TERSat CDR Structural Model 75
5.6 Monte Carlo Analysis of TERSat PQR Structural Model 78
5.7 Sensitivity Analysis of TERSat Structural Model 78
5.8 Conclusion of Finite Element Analysis Uncertainty Propagation . . . 83

6 Lessons from the TERSat Prototype **85**

6.1 Changes to the outside of the TERSat design 85

6.1.1 Solar Panels 86

6.1.2 Development of Miscellaneous Brackets for Non-structural Elements 87

6.2 Changes to the inside of the TERSat design 87

6.2.1 STACER Mounting Bridge 87

6.2.2 Power Distribution System Design 87

6.2.3 Cable Harness Development 88

6.3 Modification of the Payload Antenna after Testing 88

6.3.1 Unit Under Test 88

6.3.2 Test Setup 90

6.3.3 Test Anomalies 90

6.3.4 Anomaly Resolution 90

6.3.5 Comments and Test Summary 90

6.4 Summary of Subsystem Design Mass Changes after As-built Prototype 93

6.5 Conclusion 96

7 Conclusion and Future Work **97**

7.1 Future Work in Input Uncertainty Characterization 97

7.2 Future Work in Studying Additional Quantities of Interest 98

7.3 Future Work in Validating Methodology with Additional Programs . 98

7.4 Summary 99

List of Figures

1-1 Traditional Spacecraft Design Approach 19

1-2 Proposed Spacecraft Design Methodology includes uncertainty propagation and sensitivity analysis to reduce the need for costly extra redesign steps late in program development 21

1-3 Examples of exponential entropy for Gaussian, uniform, triangular, and bimodal distributions 24

1-4 Photograph of the TERSat prototype 29

2-1 Setup of test system example 32

2-2 Distribution of System TRLs after improving one part/subsystem by one TRL based on two measures of uncertainty in the system showing that complexity was more effective for this test system 35

2-3 Mass Probability Density Function with Improved TRLs selected based on Mass Margin and Complexity 36

2-4 Comparison of which approach caused the greatest improvement in probability of meeting requirements, based on 1000 trials. Most of the results were ties, but of the remaining 10%, for 8% complexity was the superior guide for resource allocation 37

2-5 Continuing timesteps with each approach until each reaches a probability under 10% 38

2-6 Comparison of which approach caused the greatest improvement in probability of meeting requirements using multiple TRL improvement steps, based on 1000 trials 39

3-1 Illustration of TERSat with deployed 2.5m antenna booms 42
3-2 Illustration of interaction between TERSat and DSX 44
3-3 Overview of TERSat Prototype 46

4-1 Histograms of mass budget Monte Carlo analysis over the course of the program 57
4-2 Probability Density Functions of mass budget Monte Carlo simulation over the course of the program 58

5-1 TERSat Structural Design Summary 64
5-2 Finite Element Analysis Approach 66
5-3 Finite Element Analysis model summary 69
5-4 First mode of 101 Hz 70
5-5 Stress analysis results of ESPA interface spacecraft panel 71
5-6 Stress analysis results of the battery box 72
5-7 Revised first mode of 109 Hz 73
5-8 Histogram of Monte Carlo Analysis Results of CDR versus post-CDR 76
5-9 Probability Density Function of Monte Carlo analysis results of CDR versus post-CDR 77
5-10 Histogram of Monte Carlo Analysis Results 78
5-11 Probability Density Function of Monte Carlo analysis results 79
5-12 Probability Density Function of Monte Carlo analysis results 81

6-1 Photographs of the TERSat Prototype show the addition of smaller components 86
6-2 TERSat STACER Shake Test Unit. The STACER was secured to the shake test interface plate with clamps to simulate the mounting of the STACER to the TERSat structure. A mesh cover protected surrounding workers from accidental deployment of the STACER. . . 89

6-3 TERSat STACER Shake Test Anomaly. The STACER antenna was not adequately secured with the TERSat housing design and shook loose during testing along the axis of the antenna. 91
6-4 The addition of a stopper to the TERSat STACER test setup prevented the STACER from shaking loose during testing along the axis of the antenna. 92
6-5 TERSat STACER Shake Test, Final Configuration. The STACER assembly successfully completed the rest of the shake test. 94
6-6 Comparison between TERSat subsystem mass predictions at PQR and measured values of the as-built prototype. While there were substantial changes in subsystem masses, the sum of the changes was small (less than 2% of the CBE at PQR 95

List of Tables

3.1 Mission Statements and Success Criteria 45
3.2 TERSat Mass Budget 47
3.3 TERSat Power Budget 47
3.4 Payload Design Parameters 48

4.1 Subsystem Mass Complexities after CDR 59

5.1 Materials Data 65
5.2 Modal Analysis Results, First Iteration 70
5.3 Stress Analysis Results, First Iteration 71
5.4 Modal Analysis Results, First Iteration 72
5.5 Modal Analysis Results, First Iteration 73
5.6 Density Inputs to Finite Element Analysis 75
5.7 Sensitivity Analysis Results 82

Chapter 1

Introduction

Space programs are increasingly complex and suffer from uncertainty in many quantities of interest, leading to schedule and cost overruns. NASA's "Faster, Better, Cheaper" approach worked for some programs (for example, Stardust as described in Atkins, 2003 [3]), but for several high-profile Mars missions this approach led to failure and the aerospace industry abandoned it [17]. While many papers have been written giving statistics of cost and schedule overruns in aerospace systems, we can build on this literature by identifying practical next steps in implementing the knowledge from these statistics to efficiently manage uncertainty in space systems. As summarized by Collopy (2011), leading industry systems engineers agreed during a series of NASA and NSF workshops that uncertainty management is one of the most needed areas of research in space systems engineering [8]. According to Collopy, "Systems engineerings first line of defense against uncertainty is a semi-quantitative risk management process with no rigorous foundation in the theory or calculus of probability." [8]

We propose a methodology for spacecraft design which consists of starting with traditional system models and using these models to characterize uncertainty in model outputs with Monte Carlo simulation, sensitivity analysis, and complexity characterization to reduce the need for expensive redesign. We use the Trapped Energetic Radiation Satellite (TERSat) as a test case for evaluating this methodology.

We introduce practical methods for accounting for uncertainties in various quanti-

ties of interest. We use uncertainty analysis of mass budgets to show how to integrate the statistics of space program mass budgets with space program development. Next, the methodology is extended to more complex analysis with finite element analysis of TERSat. Finally, the TERSat lessons learned are documented to reflect on the results of program uncertainty.

1.1 Motivations for Incorporating Space Program Uncertainty Statistics

Space programs are complex systems and suffer from large uncertainties in cost and schedule. For example, a NASA study found that to obtain better than 65% joint confidence level in cost and schedule, programs need to maintain 30-50% reserve in cost budgets and schedules[23]. Such high reserves are considered politically untenable[23]. Critical quantities of interest in a program include cost, schedule, and mass margin, and these are often closely coupled. According to Karpati et al. (2012),

> Especially for satellite systems, the mass margin is intimately tied to other engineering and management goals such as performance, cost, schedule, and risk. As the mass of the object to be launched approaches the throw-mass limit of the launch vehicle, decisions by the development team skew more aggressively toward mass savings at the expense of some combination of performance, cost, schedule, or risk. Not all satellite development programs that are over their mass controls are cancelled, but the converse is usually true...that is, cancelled programs are almost always over their mass controls. [20]

The reason changes in certain quantities of interest can have such a great effect is that changes in any part of a system can propagate through a system. Giffin and de Weck (2009) studied the propagation of changes in complex systems and found that changes in components at the intersection of major functional areas have the greatest

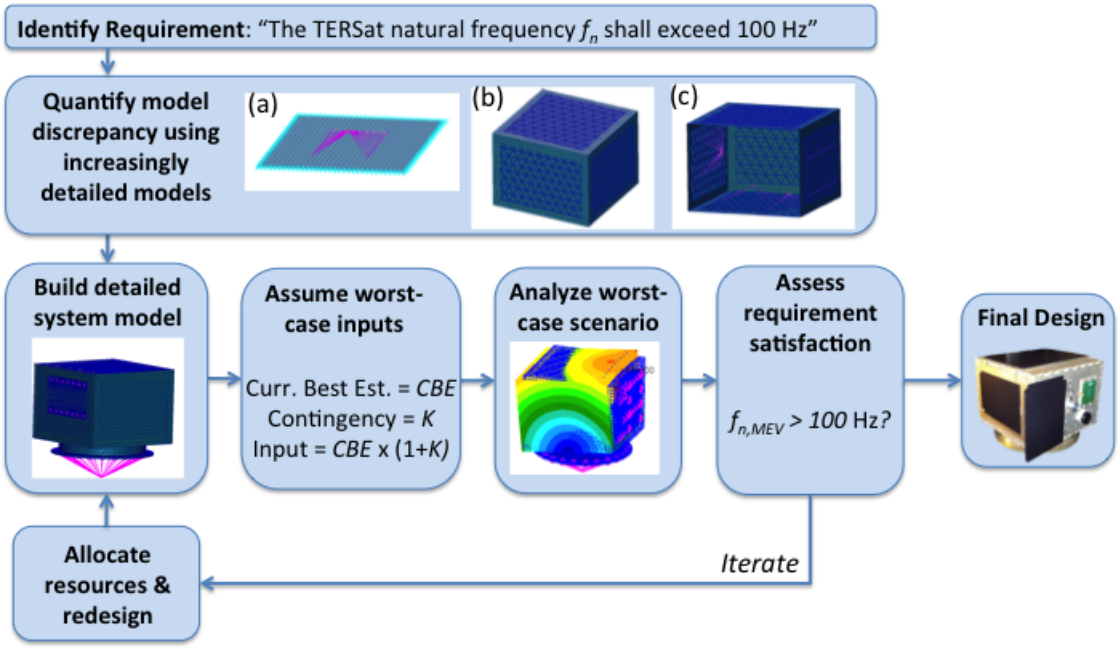

Figure 1-1: Traditional Spacecraft Design Approach

effects, but even changes in one subsystem can still affect subsystems that are not closely related on a Design Structure Matrix (DSM) [11].

Many papers have studied the historical trends of these quantities of interest in space system development. For example, Kipp presented statistics of mass, power, schedule, and cost of numerous NASA missions [21]. In this paper, Kipp et al. correlated growth in these quantities of interest with instrument type, mass, and power. Another example of statistical studies of space programs is Dubos et al. (2007), which compared technical readiness level of space systems with trends in program schedule [14]. Finally, Browning (1999) identified sources of schedule risk in complex system development [7].

These studies showed that space systems tended to increase in mass, cost, and schedule over time and they help to identify the drivers for these difficulties. However, a next step is needed to bridge the gap from the results of these papers to

implementing the knowledge in a real space system. This thesis proposes methods for incorporating uncertainty statistics in mass, natural frequency, and schedule into complex spaceflight program development.

For systems where a system of equations can fully describe the system, optimization under uncertainty is possible. For complex space systems, currently there is a limit to how much of the system can be described only by a system of equations without some human understanding in the loop. By incorporating studies of uncertainty with software tools currently in use, greater insights can be gained while maintaining practicality.

1.2 Research Objectives and Methodology

The objective of this work is to develop a spacecraft design methodology that reduces cost and schedule overruns while meeting program design requirements by identifying issues and design drivers early in development using uncertainty and sensitivity analysis of detailed system models. The Trapped Energetic Radiation (TERSat) program is used as a test case for evaluating this methodology.

The research approach was to define the methodology and then apply it to TERSat as a test case. We evaluate success based on both quantitative and qualitative measures:

- Quantitative: Demonstrate reduction in risk of failing a requirement
- Qualitative: Guide for layout fine-tuning, improved understanding of uncertainties

As illustrated in Figure 1-2, the methodology begins with requirements on quantities of interest in the system. Validated models of increasing fidelity are built to model the quantity of interest. Then, rather than making assumptions about what the worst-case scenario might be, probability distributions are determined from historical data for inputs to the models. These uncertainties are propagated in the model using Monte Carlo simulation to determine the uncertainties in the output.

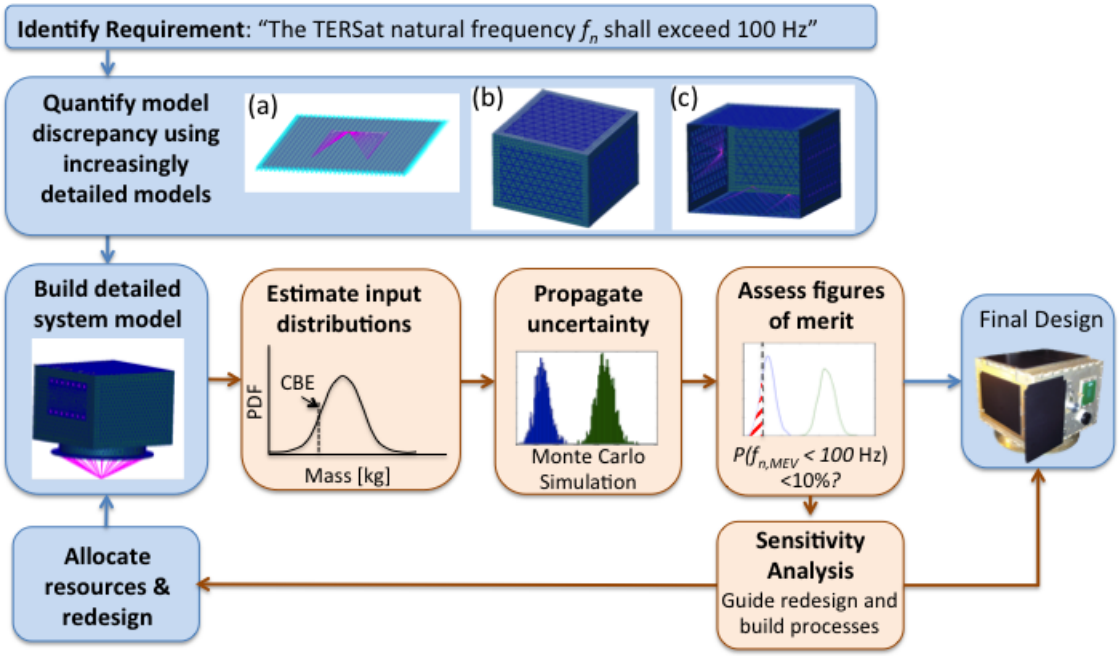

Figure 1-2: Proposed Spacecraft Design Methodology includes uncertainty propagation and sensitivity analysis to reduce the need for costly extra redesign steps late in program development

The figure of merit of this methodology is the probability of failing the requirement. Sensitivity analysis and measures of complexity can then be used to refine requirements on related quantities of interest or help in redesigning the system.

The first quantity of interest under study was the TERSat mass budget. This was selected for two reasons: (1) mass is a critical quantity to monitor because TERSat had a requirement to stay under 50 kg and (2) mass budgets are simple types of models because the numbers in the models sum linearly.

The next quantity of interest under study was the TERSat first fundamental frequency. TERSat has a requirement that the first mode must exceed 100 Hz. Finite element models using traditional margin techniques produced an expected value of 101 Hz for the baseline design, but this approach does not produce error bars on the result. Following the above methodology, the uncertainties identified in the mass budget analysis were used as inputs for the spacecraft modal analysis to show how likely it was that the satellite would meet requirements. Because the uncertainty analysis of the mass budget showed significantly higher likelihood of meeting the mass requirement than the frequency uncertainty analysis showed of meeting the frequency requirement, mass was added to stiffen the structure.

1.3 Literature Review

The literature review is focused on three areas: system complexity, system uncertainty, and current practices in space systems for managing complexity and uncertainty.

1.3.1 Measures of Complexity in Complex System Design and Implementation

According to Shalizi (2006), "a complex system, roughly speaking, is one with many parts, whose behaviors are both highly variable and strongly dependent on the behavior of the other parts." [30] However, there are many methods of defining system

complexity. In a website, Shalizi even humorously summarizes the various complexity metrics by saying "Every few months seems to produce another paper proposing yet another measure of complexity, generally a quantity which can't be computed for anything you'd actually care to know about, if at all. These quantities are almost never related to any other variable, so they form no part of any theory telling us when or how things get complex, and are usually just quantification for quantification's own sweet sake." [31]

In general, system complexity definitions fall into two categories, structural and behavioral. Structural complexity is a measure of how complex the architecture of a system is, while behavioral complexity is a measure of how unpredictable the behavior of a system is. Here we survey some of each type of metric. The exponential entropy metric was selected for use in the methodology we present.

Behavioral Complexity Metrics

Behavioral complexity draws from information theory. There are several definitions. Kolmogorov defined complexity based on the amount of entropy in a string [22]. Arthur Ferdinand defined complexity as a measurement of the errors in a system, in which a perfectly simple system has 0 complexity and no errors [2]. The META exponential entropy complexity metric from Willcox et al. (2011) is derived from the concept of differential entropy from information theory [39]. Differential entropy is defined as:

$$h(X) = -\int_{\Omega_x} f_x(x) \log(f_x(x)) dx \tag{1.1}$$

For example, for a uniform distribution spanning a to b, the differential entropy is $\ln(b-a)$. The exponential entropy metric defines complexity as:

$$C(Q) = e^{h(Q)} \tag{1.2}$$

Thus, the units of the exponential entropy metric are the same as the units of the quantity of interest. This makes the exponential entropy metric more intuitive.

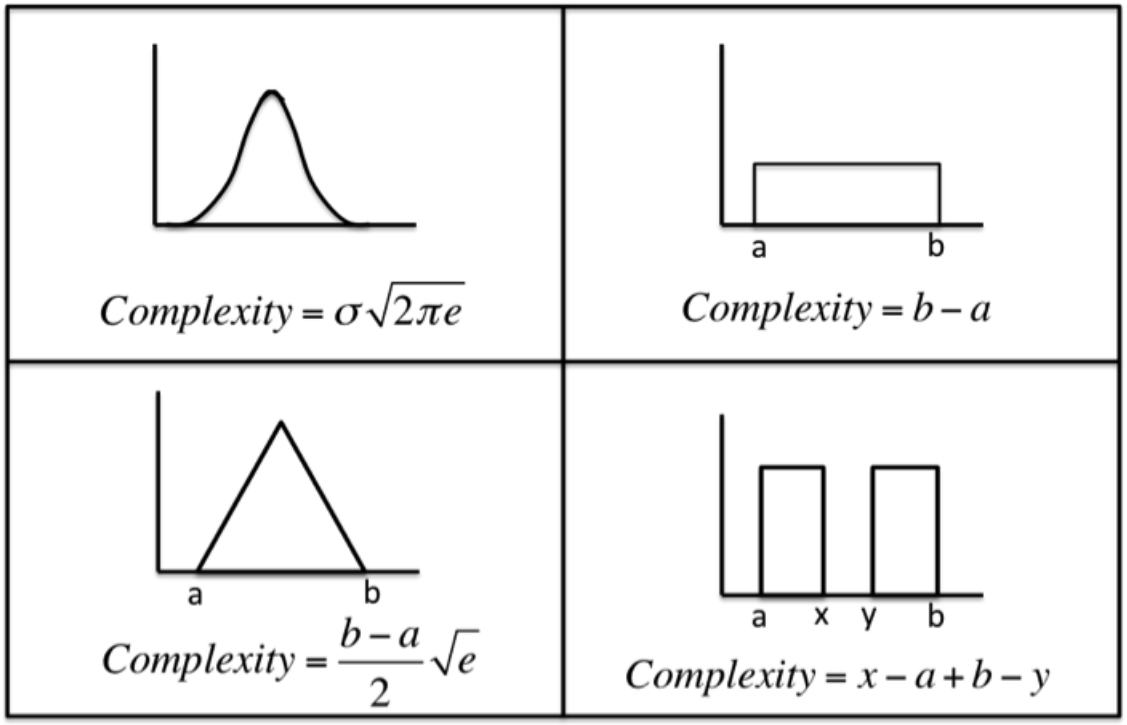

Figure 1-3: Examples of exponential entropy for Gaussian, uniform, triangular, and bimodal distributions

For example, for a uniform distribution, the exponential entropy is simply b-a. Some examples of distributions and their complexities are shown in 1-3.

Structural Complexity Metrics

de Weck and Murray (2011) [25] present an example of structural complexity that uses a combination of complexity terms. In this work, complexity is composed of three parts: structural, dynamic, and behavioral. These three terms are multiplied together to achieve an overall system complexity.

The structural complexity term is based on graph theory, in which the components of the system are nodes and component interfaces are edges of the graph. This definition is derived from the measure of energy of molecules.

The dynamic complexity is related to Shannon entropy, similar to the exponential entropy metric, but in this case dynamic complexity measures the interdependence of different quantities of interest in the system.

Another definition of complexity, specifically developed for space systems, is the Bearden (2003) model which relies on twenty one factors including design life, max distance from Earth orbit, ADCS type, and number of payload instruments. This complexity metric is used to determine the risk of pursuing an interplanetary mission since these have constrained schedules [4].

Complexity Metric Selection

Each of these measures of complexity is useful for different applications. For understanding uncertainty, behavioral complexity is the most relevant complexity metric. The exponential entropy complexity metric offers a measure of complexity with convenient units and useful response to discrete alternatives. This definition provides a complement to standard deviation as a measure of uncertainty and was selected for this methodology.

1.3.2 Uncertainty of Quantities of Interest in Complex System Design and Implementation

According to [5], there are three categories of uncertainty:

- Aleatory Uncertainty: This type of uncertainty represents the random errors in a system. On a target, this type of uncertainty represents the distribution, or precision, of the hits.
- Epistemic Uncertainty: This type of uncertainty represents systematic uncertainty in a system. In the example of a target, this represents the accuracy of the hits.
- Ambiguity: This represents a lack of system knowledge and behaves similarly to epistemic uncertainty.

Part of the META approach to systems engineering is that system uncertainty should be quantified and tracked throughout the systems engineering process. Under the META approach, both aleatory and epistemic uncertainty are combined into probability density functions. Sondecker (2011) went as far as describing how to identify quantities of interest to use in the META framework, but did not implement the META complexity evaluation [33]. We take the next step by performing uncertainty analysis on spacecraft quantities of interest.

1.3.3 Notes on Optimization

Optimization is related to the topic of uncertainty analysis of complex systems. Some optimization problems deal with uncertainty of complex system design. Robust optimization and stochastic optimization are related to this field.

Stochastic optimization uses random variables to represent inputs in the setup of optimization problems. The goal of stochastic optimization is to find a good result with uncertain inputs using efficient computing. Similarly, robust optimization attempts to find an optimal solution that is optimal for a range of inputs. In contrast, deterministic methods fully sample a space, but this is inefficient for complex systems.

In complex system design, optimization is often not the correct problem description. In most cases, space systems need to achieve certain requirements such as mass, but it is not necessary to reach an absolute minimum mass to be successful. Thus, simply characterizing the uncertainty through Monte Carlo analysis and using sensitivity analysis to help determine resource allocation may be sufficient to address design issues without optimization.

However, these methods are not commonly used for complex multidisciplinary systems such as space system design because these methods require a problem structure that is not widely found in these systems. Therefore we did not apply optimization to this methodology.

1.3.4 Current Practices in Complex Space System Uncertainty Management

The most typical way uncertainty is accounted for in systems engineering is through margin and contingency. Karpati et al. (2012) provides an excellent summary of margin and contingency in space systems and provides guidelines for treatment of each by subsystem. There are also standards for accounting for margin. For example, the leading standard for mass margins is AIAA S-120-2006. Margins are difficult to account for because both under and over allotment of margin can lead to problems in program development. According to Karpati et al. (2012)

> If a project takes on overly conservative margins at the beginning of a program, they may have let some mission performance go unrealized, or put themselves in an early decision to use expensive lightweight materials or risky lightweight technology. But projects that take margins that are too low walk the path of many developments where margins erode before launch and even more costly (or risky) late design trades must be made. [20]

However, this traditional method of margin management is limited in capability. It treats all uncertainties as a uniform probability distribution and does not account for the more detailed statistical results of studies like Browning's. Emmons approaches this problem and provides helpful general strategies for reducing cost and schedule overruns, such as developing instruments before developing the spacecraft to avoid costs of "marching armies" when instruments are delayed [15].

Some new approaches in systems engineering allow space systems engineers to make architecture decisions with uncertainty in mind. Silver and de Weck (2007) developed "Time-Expanded Decision Networks" which allow a systems engineer to select more flexible architectures to account for uncertainties in the system [32].

de Weck's 2006 paper on Isoperformance is another example of designing under uncertainty. In this paper, de Weck showed that optimization problems can return not just a single optimal point but a family of performance-invariant points that

can be compared by cost or other criteria [13]. Some people treat system design as an optimization problem, as Croisard (2010) did when using Evidence theory in optimizing the wet mass of the BepiColombo mission [10]. Wertz treats uncertainty in a system as a risk that can be traded with productivity. Wertz uses Markov chains to represent the chain of events of experiments, and simulates the performance loss with each ordering of experiments based on the risks of each experiment [38].

The most widespread new technique for uncertainty management in aerospace is the Joint Confidence Level technique used at NASA. This approach requires programs to demonstrate 30-50% reserves in cost and schedule. This has spurred some research in how to use Monte Carlo analysis for characterizing uncertainty in cost and schedule, such as Cornelius (2012) [9]. This technique can be extended to other quantities of interest, as we demonstrate in this thesis.

1.4 TERSat Program Summary

The Trapped Energetic Radiation Satellite (TERSat) is a 32 kg student-built nanosatellite developed under the University Nanosatellite Program (UNP). The TERSat program began in the fall of 2010 and a prototype was completed in January of 2013. The TERSat program will investigate how VLF waves interact with the radiation environment in Low Earth Orbit (LEO) by deploying a 5 m dipole, using a transmitter to radiate VLF waves over a range of voltage levels up to at least 600 V, frequencies from 350 kHz, and a range of magnetic field orientations. TERSat will also measure the strengths of the echoes with a low noise VLF receiver. A photograph of the TERSat prototype is shown in Figure 6-1.

Performing these experiments will help determine how well a deployed antenna system can overcome the antenna sheath impedance to radiate at VLF frequencies in the LEO plasma environment, how efficiently can VLF energy be radiated at LEO altitudes, and if we can explain the up to 1000 times (20 dB) model vs. observational differences in Starks et al. (2008). These experiments will be critical to the success of future missions to use VLF emissions for radiation belt remediation. The TERSat

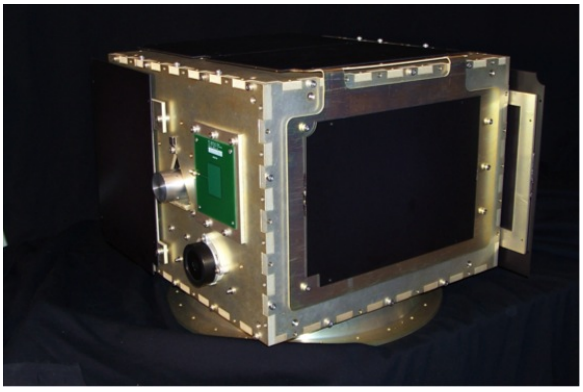

Figure 1-4: Photograph of the TERSat prototype

experiments will also allow scientists to better calibrate underlying plasma physics models which have orders of magnitude uncertainties for geometries at LEO altitudes.

TERSat's requirements derive from the UNP requirements and from the two mission statements:

MS1 Demonstrate and characterize transmission of low frequency (VLF) waves in the inner Van Allen radiation belt over a range of frequencies, over a range of power levels, and over a range of orientation to the magnetic field.

MS2 Demonstrate the ability to receive echoes/reflected signals resulting from the transmitted pulses using an on-board VLF receiver.

There are many technical performance measures that are derived from these requirements, including mass, power, and natural frequency. We focus on mass and natural frequency as the quantities of interest in the TERSat structural design test case for evaluating our proposed methodology.

Chapter 2

Methodology

This chapter describes in greater detail the methodology for characterizing uncertainty and complexity of quantities of interest. The methodology follows a bottom-up approach, first studying the uncertainties of individual inputs to models of quantities of interest. Next, these are incorporated into a model of the quantity of interest. For example, the model of the natural frequency of a spacecraft would be the finite element model of the spacecraft. Lastly, Monte Carlo simulation and sensitivity analysis show the relative importance of different parameters to complex models. A test system is described in this chapter to illustrate the methodology.

2.1 Test System Setup

To illustrate this methodology, a test system can be used as a simple, generic example of a system. A single quantity of interest, in this case system mass, has inherent uncertainties due to uncertainties in the masses of the subsystems. Typically, if uncertainty is even considered, items with larger mass growth allowance are targeted for uncertainty reduction resources. The proposed methodology employs the exponential entropy metric instead.

In the most basic test system setup, resources are allocated to increase the technical readiness level (TRL) of a subsystem by one. In one case, the subsystem with

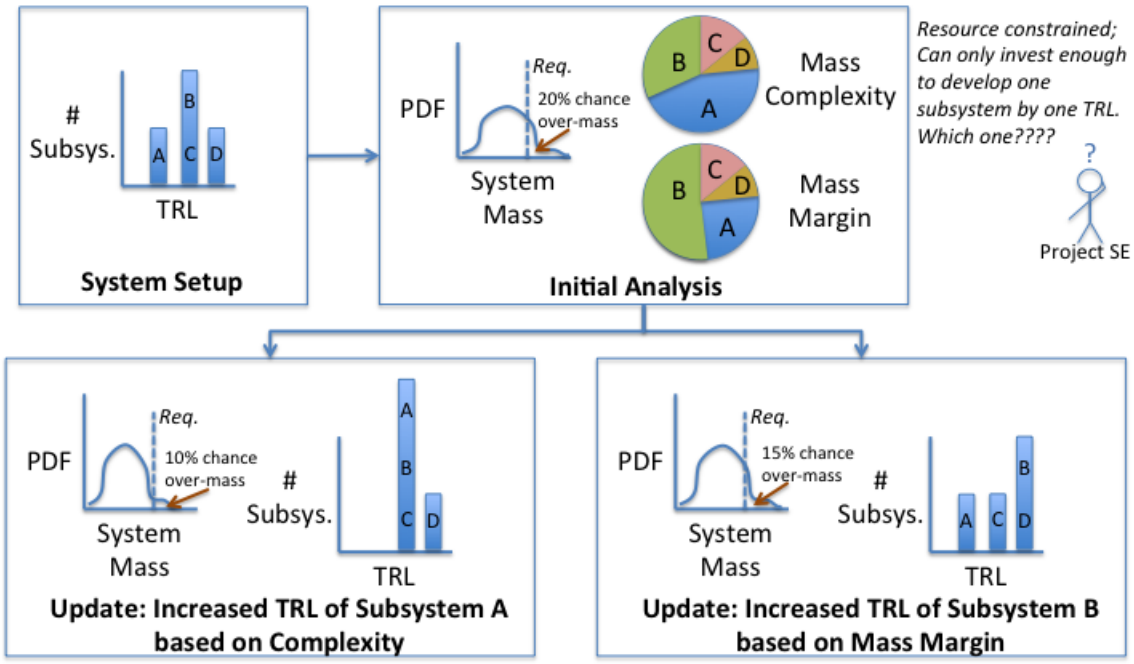

Figure 2-1: Setup of test system example

the largest mass margin is targeted, while in the other case the subsystem with the largest complexity is targeted. This is illustrated in Figure 2-1.

To set up the problem, the system is assigned some parameters: number of parts/subsystems, distribution of TRL, and order of magnitude of mass. Then a list of subsystems are generated based on these parameters. Each subsystem has a TRL (randomly assigned using the program TRL distribution shape and with for the random number generation), a mass (randomly generated within 50% of the mass order of magnitude value), and a margin, which is determined by the TRL the subsystem has been assigned. This allows a variation in subsystems with each run of the analysis, enabling Monte Carlo analysis.

Next, the subsystem masses are compiled into mass probability density functions. To do this, many masses for each subsystem are generated using the mass margin to bound the uncertainty of the subsystem. In this illustrative example, subsystems with

higher TRLs use triangular distributions to account for engineers' greater certainty in the subsystem design, while subsystems with lower TRLs have uniform probability density functions. (For reference, the actual mass budget simulation chapter uses different PDFs based on actual historical data).

These lists of subsystem masses are then compiled into histograms. Kernel Density Estimation (KDE) allows these to be turned into probability density functions, which are then used to compute complexity. To perform the KDE, the built-in KDE function in the Python SciPy package is used. This method assumes gaussian distributions for the kernels and uses the Scott rule of thumb method for determining the bandwidth of the distributions. According to Zucchini (2003), the shape of the kernel distribution does not have a significant effect on the KDE output [40]. The Scott rule of thumb is commonly used in cases of less than five dimensions, which this is [29].

These PDFs from the KDE are binned and each bin and probability density are integrated to find the complexity per Equation 1.2.

Now the system has both margin and complexity for each subsystem. Subsystems with larger margins and complexities are more uncertain that subsystems with lower margins and complexities. In the automated test system, the subsystem with the higher margin and complexity are selected for improving the subsystem TRL. Performance of each is then estimated by assuming a reference value for a requirement and determining the improvement in probability of meeting the requirement using each technique.

This test system has limitations. By automating every step, the intuition of the system engineer is removed. Interactions between subsystems are known to the systems engineer but automatically tracking and updating these interactions and their related uncertainties is outside the scope of this thesis. In a real program, which will be illustrated in later chapters, the systems engineer would use the complexity information to inform decision making in combination with the other information the system engineer has. Additionally, in a real world setup, TRL improvements can happen in parallel.

Other limitations are more technical. This test model assumes that resources to

improve a subsystem by one TRL are equal, regardless of subsystem or initial TRL. Presumably this is not the case, as transitions between some TRL numbers require building of simple prototypes, while other transitions require significant field testing.

2.2 Test System: One Timestep Example

The first test system demonstration is of taking one TRL improvement step. The test system code randomly generates a TRL distribution for a system based on inputs regarding likelihood of each subsystem TRL. Figure 2-2 shows an initial TRL distribution and the TRL distributions following the differing TRL improvement steps recommended by the mass margin uncertainty and complexity methods. Here, the complexity approach recommended improving one of the TRL 7 subsystems to TRL 8, while the mass margin approach recommended improving a TRL 5 subsystem.

The mass probability density functions of these TRL distributions are shown in Figure 2-3. While both mass margin and complexity approaches reduced the system mass uncertainty, the complexity approach was slightly more effective for this case in shifting the system mass curve to the left and reducing the standard deviation of the curve.

While in this example, complexity and margin approaches recommend different subsystems for TRL improvement, in many runs the two approaches recommend the same subsystem. As shown in Figure 2-4, a study of 1000 runs with these baseline inputs found that approximately 90% of the time complexity and margin recommend the same subsystem for TRL improvement. 8% of the time Complexity recommended a better course of action for TRL improvement than did Margin, measured by which subsystem TRL change caused greater improvement in probability of meeting the system mass requirement.

This is as expected. Complexity accounts for the shape of the distribution changing as the subsystem uncertainty decreases with increasing TRL, while margin only accounts for the width of the distribution.

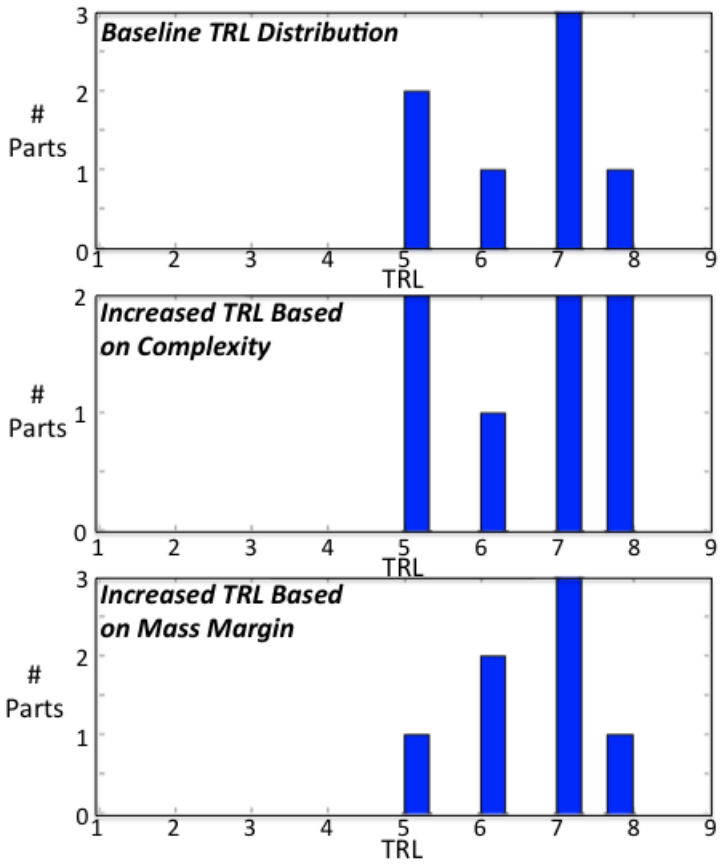

Figure 2-2: Distribution of System TRLs after improving one part/subsystem by one TRL based on two measures of uncertainty in the system showing that complexity was more effective for this test system

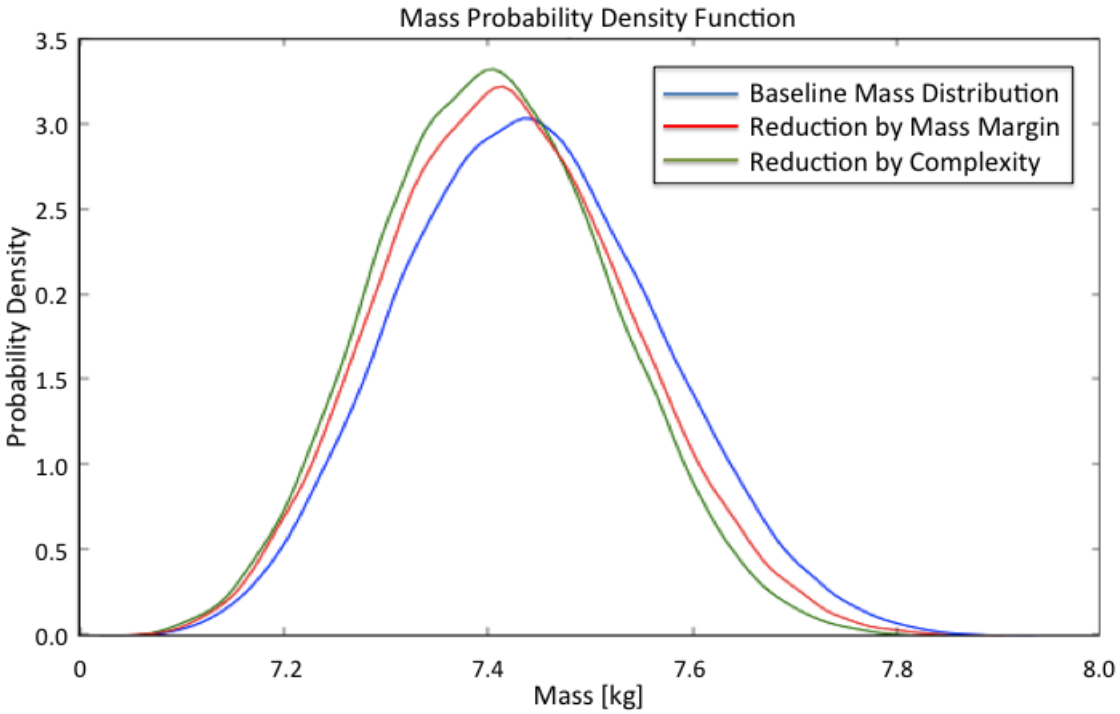

Figure 2-3: Mass Probability Density Function with Improved TRLs selected based on Mass Margin and Complexity

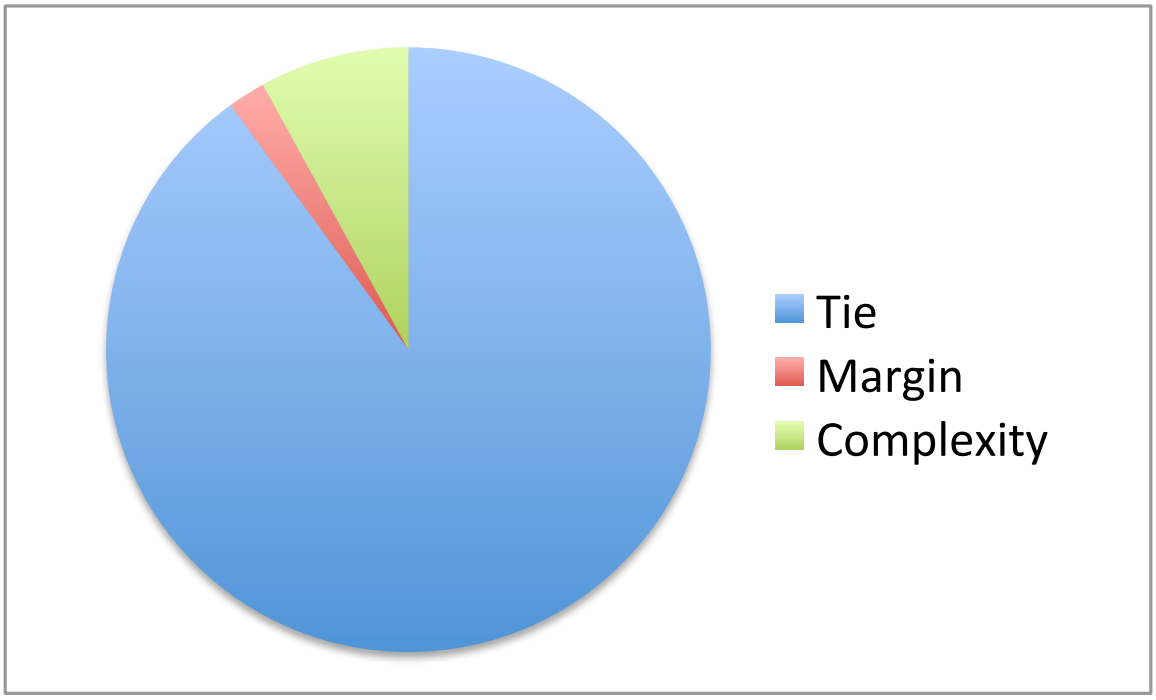

Figure 2-4: Comparison of which approach caused the greatest improvement in probability of meeting requirements, based on 1000 trials. Most of the results were ties, but of the remaining 10%, for 8% complexity was the superior guide for resource allocation

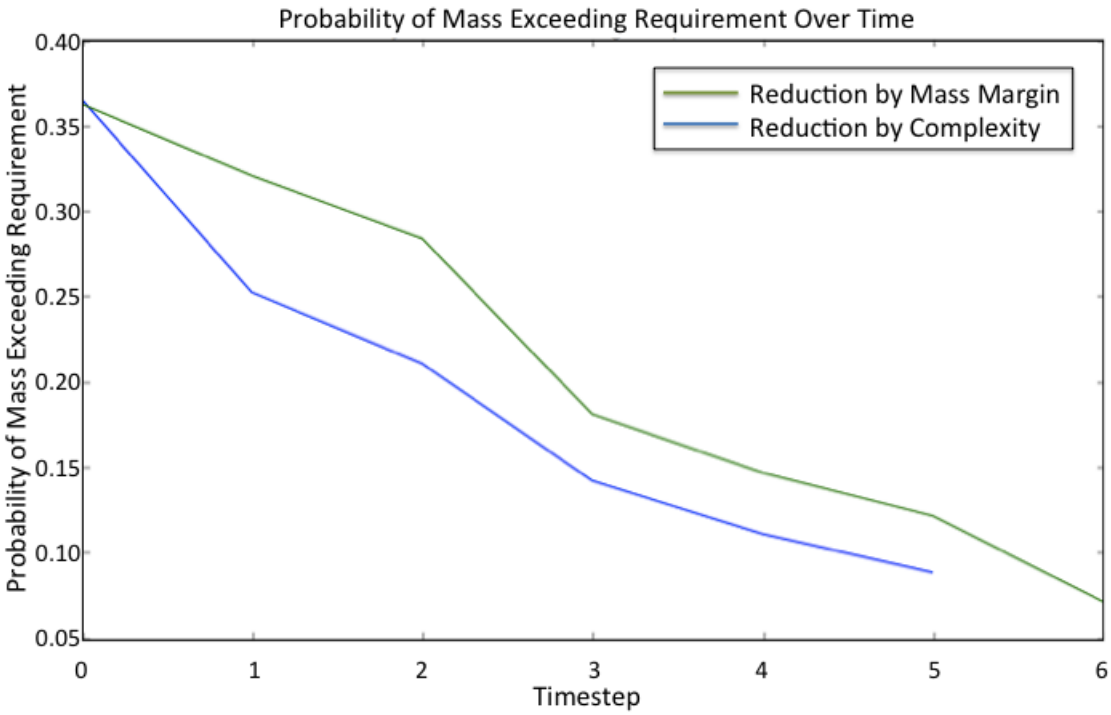

Figure 2-5: Continuing timesteps with each approach until each reaches a probability under 10%

2.3 Test System: Continuing Timesteps Example

To further illustrate this point, the test system can also be run for many timesteps to see which approach reduces uncertainty most effectively with the least resources. Figure 2-5 shows an example. In this case, complexity proved to be a more effective approach to reducing uncertainty in the test system's mass distribution than mass margin. While both approaches reduced the probability of failing the mass requirement, the complexity approach was able to reduce the probability to under 10% with fewer steps than the mass margin approach required. In the real world, this would translate to fewer resources being required to reduce system risk.

In this example, the complexity approach is more effective than mass margin at reducing uncertainty in the system. However, in many cases the two approaches show roughly the same rate of improvement.

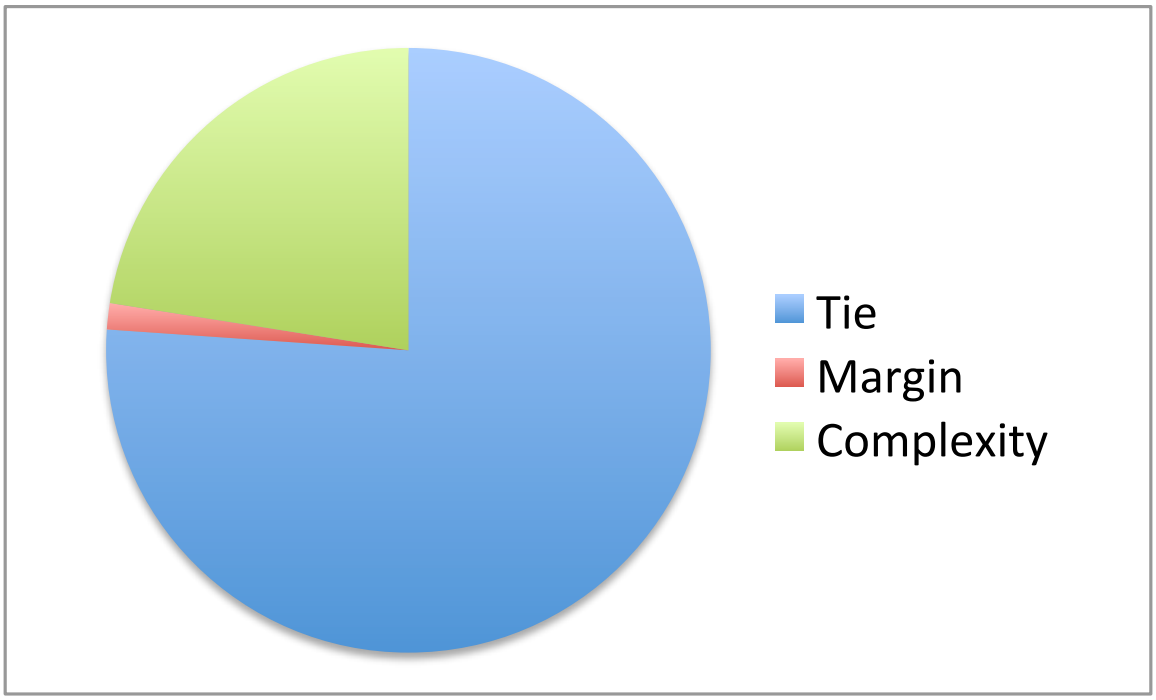

Figure 2-6: Comparison of which approach caused the greatest improvement in probability of meeting requirements using multiple TRL improvement steps, based on 1000 trials

Figure 2-6 shows that 76% of the trials resulted in a tie, with both approaches requiring the same number of steps to reach 10% probability of failing requirements. In 23% of the trials, complexity required fewer steps than margin to reduce the probability of failure to within 10%, and in only 1.4% of trials margin produced the better course of action.

These results show that most of the time, either approach will work, when the two differ complexity gives the better result. Of course, this hinges on inputs. A sensitivity analysis is required to determine what factors influence these percentages.

2.4 Test System: Parameter Variation

There are several factors that this analysis is sensitive to.

- *Shape of distributions based on TRL:* The analysis is based on assumptions about how the shape of the subsystem-level probabilities change with improve-

ments in TRL, but knowledge of the shape of these distributions is poor.

- *Distributions of subsystem TRL for the current baseline:* Could the utility of the tool vary with how developed the system is?

- *Relative subsystem mass properties:* The mass properties currently only vary by +/- 25%, but a wider distribution could skew results universally towards the heavier system.

- *Stage in design (whether or not discrete architecture trades are open):* Mass margin is not well defined for subsystems with open architecture trades, while this can be simply represented by a multimodal distribution in complexity analysis. Various mass margin approaches will be compared with the complexity analysis results.

The test system example could be carried out to investigate each of these. However, the simple example is only used to demonstrate the methodology, so we will proceed to answer these questions with the TERSat case study.

Chapter 3

Overview of the TERSat Program

Radiation damage caused by interactions with high-energy particles in the Van Allen Radiation Belts is a leading cause of component failures for satellites in low and medium Earth orbits (LEO, MEO). Strong solar storms can cause significant increases in radiation levels in the Van Allen belts leading to severe damage to nearby satellites and a significant reduction in satellite life expectancy. Solar storms and coronal mass ejections can also cripple or permanently disable spacecraft. Shielding against such events can increase the cost of space mission due to the additional mass and is not always even effective. However, it has been suggested that emissions of Very Low Frequency (VLF) waves could dissipate electrons from the radiation and mitigate the bulk of satellite exposure to intense radiation events [26].

Very Low Frequency (VLF) electromagnetic waves have been shown to couple energy to high-energy radiation belt electrons and change their properties. VLF waves from lightning and plasma hiss from magnetospheric reconnection can scatter the pitch angle of high-energy particles, such that they rejoin the neutral lower atmosphere [18]. Due to the ionospheric plasma cutoff frequency limiting the efficiency in coupling VLF from the ground to space, it has been proposed that space-based antennas transmitting VLF waves could similarly help reduce the effects of radiation by scattering electrons.

However, the interaction between a VLF transmitter and the plasma environment is not sufficiently well understood. For example, Starks et al. (2008) summarizes how

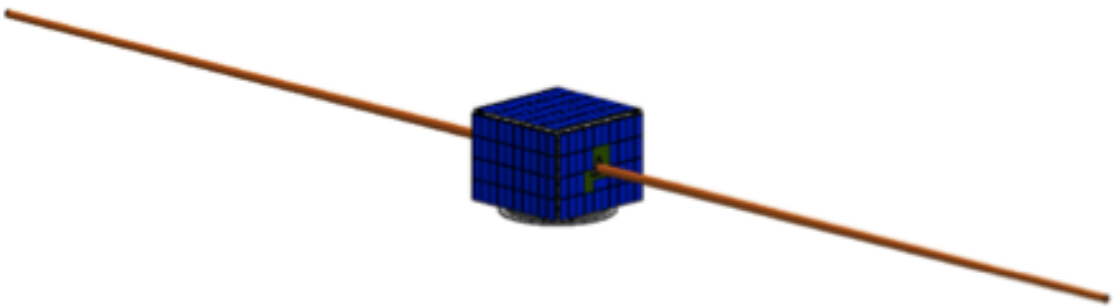

Figure 3-1: Illustration of TERSat with deployed 2.5m antenna booms

models of field strength in the plasmasphere away from the magnetic equator appear to be overestimated by a large amount, 10-20 dB, and underestimated by 15 dB at the magnetic equator for L less than 1.5. The implication is that there are important physics not understood or captured in the ionosphere and LEO altitudes [34].

It is clear that on-orbit experimentation and demonstration are needed to analyze how best to tune and couple VLF energy to the electrons and ions even though terrestrial VLF equipment is well understood and low-risk.

The Trapped Energetic Radiation Satellite (TERSat) is a 32 kg student-built nanosatellite that will analyze how VLF waves interact with the radiation environment at 550 km altitude by deploying two 2.5 m antennas to form a 5 m dipole, using a transmitter to radiate VLF waves over a range of voltage levels up to at least 600 V, frequencies from 350 kHz, and a range of magnetic field orientations. TERSat will also measure the strengths of the echoes with a low noise VLF receiver.

The TERSat science mission complements that of AFRLs Demonstration and Science Experiments (DSX) satellite. TERSat will perform a subset of the DSX experiments at a much lower orbit, giving insight into the effects of altitude-dependent plasma density and magnetic field strength on the wave-particle interactions. TERSat is also capable of interacting with DSX for bistatic experiments if the mission periods overlap. A CAD image of TERSat is shown in Figure 3-1.

TERSat will support technology development of systems that can interact with

and potentially reduce Van Allen Belt radiation by improving our understanding of transmitting and receiving VLF waves in a LEO satellite plasma environment.

3.1 Mission Overview

The Trapped Energetic Radiation Satellite (TERSat) is a student-designed nanosatellite ($\leqq$ 50 kg) that will investigate the ability of space-based Very Low Frequency (VLF) radio transmission to reduce the population of harmful high-energy particles in the inner Van Allen radiation belts. TERSat was conceived and first developed as MITs entry into the AFRL University Nanosatellite Program (UNP) competition and received design and engineering model support from UNP and NASA JPL. To date, TERSat has completed UNP-7s preliminary design review (PDR), critical design review (CDR), the pre-prototype build Proto-Qualification Review (PQR), and the flight competition review (FCR). On June 30, 2012, TERSat flew a prototype VLF transmitter and tested their ground station receiver as a participant in AFRLs Student Hands On Training (SHOT II) high altitude balloon experiment.

TERSat will radiate VLF waves and measure the strength of the echoes. TERSat could also receive echoes from DSX transmissions, and could transmit for detection by the DSX receiver. The bus and deployed antennas are illustrated in Figure 3-1. TERSats baseline orbital altitude is 550 km, but altitudes up to 600 km will still satisfy the UNP de-orbit requirement and are thus acceptable.

Experiment parameters: TERSat will radiate VLF waves at 3, 25, and 47 kHz, 100, 300, and 600 V, and orientations of perpendicular, 45 degrees, and parallel to the magnetic field lines. TERSat will start with lower voltages and step up to at least 600 V due to uncertainty in the voltage at which arcing begins to occur.

A possible addition to the experiment plan would be to interact with the AFRL satellite DSX. Such an interaction would add an additional dimension to the wave-particle interaction measurements. According to Bortnik (2002), VLF waves not only travel and reflect along one magnetic field line, they also travel radially around and along other magnetic field lines [6]. This would allow TERSat and DSX to monitor

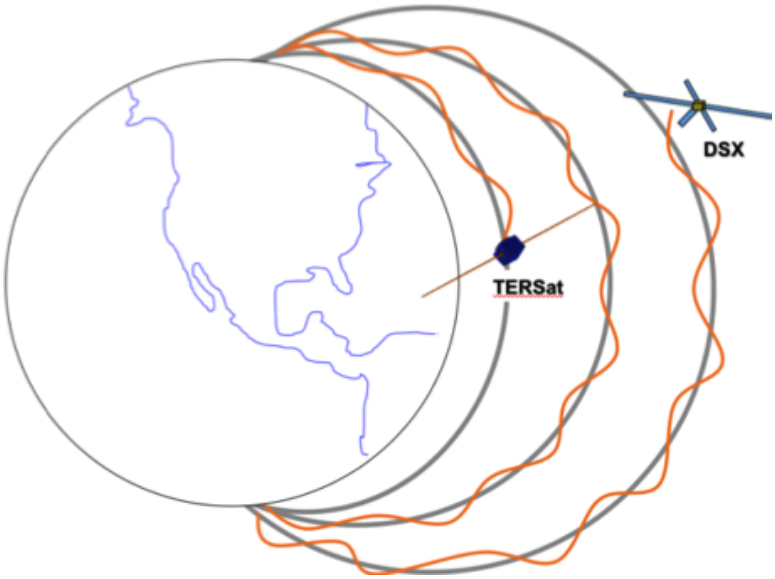

Figure 3-2: Illustration of interaction between TERSat and DSX

each others transmissions and provide a better understanding of radial VLF wave propagation. This interaction is illustrated in Figure 3-2. The orange curve indicates the VLF waves motion along the magnetic field lines. As noted by Bortnik (2002), the ability of a VLF wave to move radially has a dependence on transmitted frequency [6].

Additionally, because plasma density and magnetic field strength varies with orbital parameters and altitude, TERSat could repeat DSX experiments to provide an understanding of how the density and field strength variations affect VLF propagation.

3.2 Requirements and Success Criteria

The TERSat Mission Statements are shown in Table 3.1. To be successful, TERSat must accomplish both of the minimum success criteria: (i) transmit and characterize how effectively a VLF pulse is launched perpendicular to the local magnetic field, and (ii) receive VLF signals using an on-board receiver.

The objective success criteria characterize the effects of frequency, voltage (power) and magnetic field orientation on how well VLF waves interact with electrons in

Table 3.1: Mission Statements and Success Criteria

Statement	Description
MS1	*Objective Success Criteria:* Demonstrate and characterize transmission of low frequency (VLF) waves in the inner Van Allen radiation belt over a range of frequencies, over a range of voltages, and over a range of orientations to the magnetic field. *Minimum Success Criteria:* Demonstrate and characterize transmission of low frequency (VLF) waves in the inner Van Allen radiation belt near 50 kHz, at one voltage, with an orientation perpendicular to the magnetic field.
MS2	*Objective Success Criteria:* Demonstrate the ability to receive echoes/reflected signals resulting from transmitted pulses using an on-board VLF receiver. *Minimum Success Criteria:* Demonstrate the ability to receive VLF signals using an on-board VLF receiver.

plasma. The minimum success criteria address a more basic but still critical science question: can a deployed antenna system overcome the antenna sheath impedance to radiate at VLF frequencies in the LEO plasma environment? Self-monitoring of the relative phase between the voltage and current on the transmitter should provide insight as to whether effective transmission occurs (if the voltage and current are in-phase, the system is well-matched). It is important to demonstrate the independent functionality of the VLF receiver by measuring other (natural or man-made) VLF signals in addition to any received self-echoes. For example, this would be useful if a reasonable match is measured at the transmitter and yet no self-echo is received.

3.3 Design Overview

TERSat is a 41 x 41 x 30 cm satellite with an as-built prototype mass of 32 kg. The TERSat payload will deploy two 2.5 m STACER antennas, transmit VLF waves using a student-designed and fabricated transmitter, and measure the strengths of the echoes and other VLF signals with a Stanford VLF receiver identical to the DSX receiver. The solar panels consist of donated solar panels from Vanguard and are body-mounted on five of the six outer structural panels. All electrical components are

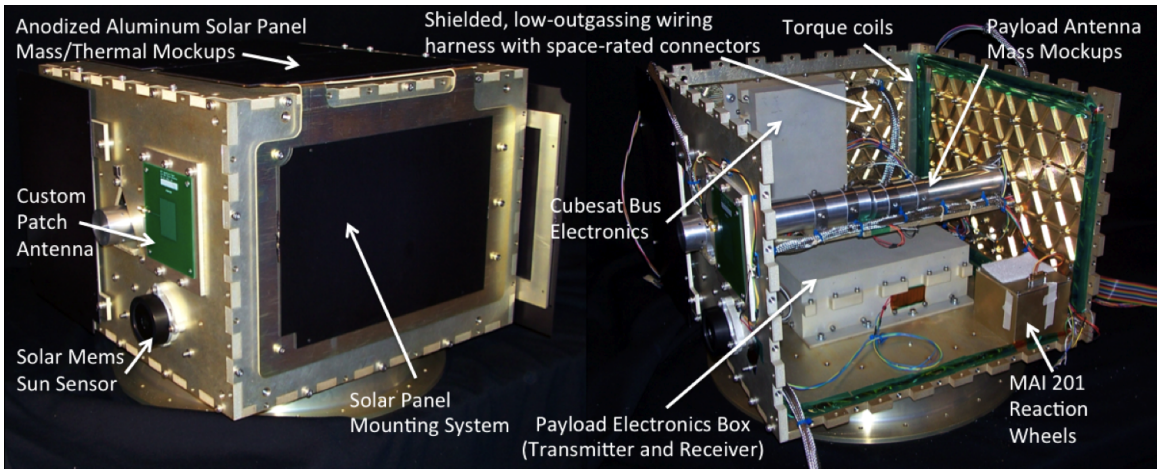

Figure 3-3: Overview of TERSat Prototype

contained within the aluminum 6061-T6 chassis, including the batteries, computer, communications, and power electronics. The Attitude Determination and Control System (ADCS) uses three reaction wheels in conjunction with three customized torque coils. The spacecraft walls consist of skinned isogrid Al6061-T6 panels. Placement of these components is shown in Figure 3-3.

TERSat bus electronics take advantage of CubeSat technology, including a Pumpkin Motherboard and processor, a Clyde Space EPS, and an MHX S-band communication system. This enables standardization of interfaces and reduced wiring needs for rapid design and integration. It also reduces the qualification testing associated with custom parts.

3.4 Technical Performance Measures

The TERSat Program has tracked technical performance measures including mass, power, data, and communications budgets to ensure design success. A master equipment list (MEL) has also been used to keep track of all system components.

As shown in the PQR mass budget in Table 3.2, the structures subsystem dominates the mass of TERSat. To ensure structural stability under earlier high uncertainty of other subsystems, the structure was over designed. The panels are formed of

isogrid aluminum rather than a more weight-efficient composite-honeycomb sandwich design to reduce complexity.

Table 3.2: TERSat Mass Budget

Subsystem	Subtotal [kg]	Margin	Mass Budgeted [kg]
Structures/Thermal	14.6	15%	16.8
Avionics/Comm.	3.03	15%	3.5
ADCS	1.00	15%	1.15
Power	6.72	25%	8.40
Wiring	3.00	50%	4.5
Payload	4.88	25%	6.10
System Subtotal	33.2	System Total	40.4

The TERSat power budget is shown in Table 3.3. In most modes, the thermal subsystem dominates TERSat power usage. Heaters protect temperature-sensitive components such as batteries when the rest of TERSat does not produce enough power to compensate in heat production.

Table 3.3: TERSat Power Budget

Subsystem	Commissioning	Nominal	Payload Tx	Safe Mode
Comm	4.6 W	0.9 W	0.3 W	4.6 W
Avionics	2.5 W	2.5 W	2.5 W	2.5 W
ADCS	2.8 W	3.5 W	4.0 W	0.4 W
Thermal	7.5 W	7.5 W	0.0 W	7.5 W
Power	2.1 W	1.7 W	1.5 W	0.9 W
Payload	0.2 W	0.0 W	40 W	0.0 W
Total	19.9 W	16.2 W	48.2 W	16.0 W

One interesting feature of the power budget is the payload power during operation. While transmitter power can be estimated based on the plasma interaction models, only the input voltage (100-600 V) can be known with certainty as the radiated power depends on how well the transmitter circuit is tuned to the plasma environment, which cannot be known or adjusted until experiments commence on-orbit. Measurement and characterization of the power drawn is one of the expected results of the experiment.

3.5 Payload Design

The TERSat payload consists of three key elements: the STACER antennas, the VLF transmitter electronics, and the Stanford Wave-induced Precipitation of Electron Radiation (WIPER) VLF receiver. The transmitter electronics and the receiver each have a dedicated chassis, and although electrically connected, the STACER antennas mount to opposite panels to create a dipole when deployed. The payload design parameters were selected using a Matlab simulation of electromagnetic radiation in a plasma. The simulation predicts the expected power output for a range of inductance values assuming a 600 V input. As the inductance values were tuned from 0.3 H up to 1 H, the power output and resonant frequency of the circuit varied.

The final design parameters are shown in Table 3.4. The antenna length of 5 m was found to be sufficient for experimental needs while still short enough to be easily accommodated by existing facilities when deployed for testing. A peak voltage of 600 V is expected to provide sufficient margin on the minimum voltage of arcing in plasma.

Table 3.4: Payload Design Parameters

Parameter	Value
Antenna Length	5 m
Peak Voltage in	600 V
Frequency Range	3-50kHz
Inductance Range	0.2-3.0 H

For the antenna, the STACER system developed by Ametek Hunter Spring was selected. The STACER is a coiled spring-type mechanism. For lengths less than 10 m (35 ft) the STACER can be purchased as a pop-up one-time deployment model using stored elastic energy to fully deploy. The key benefits of the STACER system are its versatility and 600 mission flight heritage. The TERSat STACER will use a conductive Beryllium-Copper alloy as it provides both structural rigidity as well as the electrical conductance needed for the science mission. TERSat has purchased a STACER and designed and machined STACER deployment structures for develop-

ment. Testing is now underway, including deployment reliability, control dynamics, and interface testing.

During payload operation, the TERSat transmitter will radiate VLF waves for 1 to 30 seconds within the range of 350 kHz. At least 600 V will be supplied from the transmitter to the antenna in order to radiate these waves. The core of the transmitter is the H-bridge circuitry, which takes power from the battery pack and a low-voltage logic signal from a microcontroller. The H-bridge will trigger off of the microcontroller pulse and continuously switch the direction of the current supplied by the batteries and form a full square wave. The output voltage will then be fed into a transformer that will be used to step up the output voltage to the desired maximum of 600 V. This stepped-up voltage will be supplied to the payload in the form of a sinusoidal waveform (using an RLC circuit to tune/impedance match, which will also filter out high-frequency components of the square wave) and will be used to radiate VLF waves. The transmitter voltage and current will be measured and their phase tracked in order to provide power estimates as well as information on the impedance match. It is important to characterize the impedance of all components in the transmitter as a function of frequency during testing. Preliminary tests of an engineering model have shown that at a low voltage and frequency, the H-bridge and transformer will be able to generate high-voltage VLF sinusoidal output.

The TERSat VLF receiver uses the Stanford WIPER VLF receiver chip. This chip has a wide bandwidth and is capable of receiving from 100 Hz to 1 MHz [24]. It is also low power, requiring less than 0.5 W to operate. This chip will be placed on a PCB with supporting electronics. EMI filtering will maintain the sensitivity of the chip and scrub the incoming signal from the dipole antenna. The receiver chip will interpret the signal and the primary avionics computer will process the data. The WIPER chip and supporting electronics will be housed in an aluminum chassis mounted to a side panel of the spacecraft.

3.6 Program Schedule

Moving forward from the AFRL UNP-7 schedule through January 2013, TERSat will transition from a heavily focused design and engineering model phase to a flight build phase. Preliminary steps for this phase have already occurred through the development of FlatSat demonstrations. During the process of ETU assembly for the UNP PQR (proto-qualification review) and FCR (flight competition review), both component and integrated functionality tests were performed on the components to assess operation and durability of the satellite. Component testing will evaluate the operation of individual components. Integrated testing will analyze the interactions between subsystems by testing communication among components, verifying correct power levels are being supplied to the subsystems and payload.

Chapter 4

Mass Budget Analysis

Spacecraft mass is a source of cost increase. Increased mass reduces margins on structural design, and this can lead to costly redesign. Additionally, mass tends to increase over the course of a program in an unpredictable way. The current approach of standard mass margins often fails to adequately predict how much the mass of a system can grow [16]. In an Aerospace Corporation study, the average mass growth of 10 systems was 43% over the course of a program, while typical industry guidelines recommend 30% reserves (both relative to Current Best Estimate, or CBE) [16]. However, increasing the reserved margin is not necessarily the answer, as designing structures and mechanisms to uniformly accomodate possible heavier systems may be unnecessarily difficult and costly.

System mass growth has several common sources, categorized as internal or external sources, according to the AIAA [35]. The internal sources of mass growth are:

- Better definition of the design (Internal)
- Out of scope (External)
- Redesign (Internal/External)
- Maturing component design (Internal)
- Error in previous estimate (Internal)

- Uncontrolled vendor changes (External)
- Mass reduction activity (Internal)
- Measured vs. calculated (Internal)
- Mass added for cost/schedule reduction (Internal)

4.1 Potential of Uncertainty Analysis to Reduce Cost and Schedule Growth

"Better definition of the original design" was found by Thompson et al (2010) to be the source of 54.5% of the total mass growth observed across a "small sample" of space vehicles [35]. Perhaps with a better characterization of uncertainties in the system mass early in design, this growth can be partially mitigated by reining in the current overdesign required for structures and propulsion systems designing under uncertainty. Performing uncertainty analysis and applying the exponential entropy complexity metric can help to identify characterize uncertainty in system mass.

Additionally, because mass budgets are such a simple model of a system, with masses of each component summing to achieve a total current best estimate of mass, this also provides an appropriate first case study of how to incorporate statistics of spacecraft uncertainty into a system model in general.

4.2 Traditional Approach

Mass budgets are commonly maintained in Excel spreadsheets. Uncertainty in the budget is accounted for with margin and contingency. The AIAA standard number AIAA S-120-200X gives a summary of recommended mass growth allowance and contingency [1]. This contains recommended margins for various subsystems, allowing differentiation between margins on wiring harnesses and mechanisms, for example. The recommended MGAs are provided for each phase of program development. de

Weck (2006) describes the traditional model of mass budget development of a complex space system [12]. Mass is estimated at each design review and contingency is added based on the AIAA specification. Once masses are estimated for each subsystem and margin and contingency is added, the margined masses are added to find an upper bound on the mass of the system. For many programs, this total system mass will be less than the maximum allowable value. Those programs that exceed the maximum allowable mass go through a redesign process to reduce system mass.

4.2.1 Literature on Space System Mass Budget Uncertainty

In addition to the AIAA mass growth allowance standard, studies show more statistics on mass growth. Kipp et al (2012) provides statistics on typical mass growth during NASA programs [21]. This study is based on 86 instruments across 32 NASA missions, and results are broken down by instrument type. This study found that the steepest increase in mass was between the start of Phase B and PDR.

Thompson (2010) performed detailed studies of mass growth over the course of 36 aerospace programs. He found that one out of three programs exceed the MEV recommended by the AIAA. Additional analysis of his data is given in Section 4.3.1.

4.3 Methodology for Uncertainty Management in Mass Budgets

First, the mass budget is developed according to traditional means. This ensures that the advantages of the traditional techniques are maintained. The output of this traditional process is a spreadsheet of the spacecraft mass budget. This spreadsheet was read in with a Python script.

Next, the mass budget is revised to include a column listing the technical readiness level of each component. For mass budgets created during the architecture selection phase, columns are added to allow different quantities of each part. For example,

in one column, there may be three reaction wheels, while in another column the architecture may contain only torque coils.

This allows the different architectures to be described in a single mass budget. The technical readiness level allows the masses to tie in current statistics on uncertainties in masses by TRL of the parts. A Monte Carlo analysis determines the effects of these subsystem uncertainties on the overall system mass.

4.3.1 Shape of the Mass Probability Density Function

A Gaussian distribution was selected to represent the shape of the mass distributions. The principal of maximum entropy dictates that the maximum entropy representation of a distribution with an unknown support is Gaussian. We considered a uniform distribution with the support spanning the current best estimate mass to the maximum expected value, but historical data indicates that mass distributions exhibit much longer tails than a uniform distribution can represent. Additionally, mass represents the sum of smaller parts, each of which has a value for mass that is its own random variable. By the central limit theorem the sum of random variables will become a Gaussian distribution for large numbers of samples.

Thompson (2010) performed a study of mass growth data from 36 aerospace programs [35]. Anderson-Darling and Kolmogorov-Smirnov normality tests were performed on the data from the Thompson study. To do this test, historical data from Thompson (2010) was read in. The mean and standard deviation were calculated and the historical data was compared with a Gaussian distribution with the same mean and standard deviation. The normality test found a p-value of 0.14. A typical cutoff for rejecting the hypothesis of normality is 0.05 or smaller, so the test indicates the data is normal. One concern with using Gaussian distributions to represent this data was that the support of the distribution is infinite so it can produce negative results, but with the proposed distribution based on the Thompson data the probability of producing negative mass samples is negligible.

The mean and standard deviation of the subsystem mass distributions are modeled based on the relation of the mean and standard deviation from the Thompson data

set to the best estimate (0 percent mass growth) and the maximum expected value from the data. The mean is equal to the current best estimate of mass plus 0.85 times the mass contingency. The standard deviation of the mass probability distribution is equal to the mass contingency divided by 2.7 so that 30 percent of the curve exceeds the MEV.

4.3.2 Monte Carlo Analysis

Next a Monte Carlo analysis is performed to determine a histogram of possible masses, and then a probability density function is developed based on the histogram. From this probability density function, uncertainties can be developed, including standard deviation and exponential entropy. The data points are generated for each part with a distribution based on the TRL of the component. These are added, sorted, and turned into a histogram. Next, Kernel Density Estimation (KDE) is used to smooth the histogram and produce a probability density function. This is then discretized and used to calculate exponential entropy. Note that in the mass budget simulations, a gaussian distribution is used.

4.4 TERSat Mass Budget Case Study

The TERSat mass budget analysis was performed at three stages in the design: during an architecture re-design phase after PDR and before and after a design change around the time of CDR. The details of the CDR design change will be described in detail in Chapter 5 with a discussion of the structural analysis, but here we will discuss uncertainty analysis of the mass budget.

4.4.1 Mass Budget Analysis of the Architecture Change Period Budget

Two months after the TERSat PDR, it was discovered that the original design (a 4 km tether antenna radiating electromagnetic ion cyclotron waves, or EMIC waves)

was not feasible. This was because EMIC wave coupling with plasma is only efficient when the antenna is parallel to Earth's magnetic field lines, and the tether would only rarely be close enough to parallel to allow coupling due to libration and gravity gradient effects.

This precipitated a change in the design. The mission switched to radiating Very Low Frequency (VLF) waves, which required a much shorter antenna. Analysis pointed to a 5m antenna length with 32 W of power coupled to the plasma.

At that point, the architecture of the bus needed to be re-evaluated. The bus had been structured to support two 2 km tethers with cold gas deployment systems. Now the large volume was unnecessary to stow the payload. However, a larger bus size would allow greater volume for solar arrays, potentially eliminating the need for reaction wheels to point solar arrays. This led to two possible architectures: one with a larger bus and solar arrays and no reaction wheels (using torque coils for attitude control), and one with a smaller bus and solar arrays but with reaction wheels. The reaction wheel architecture was selected because the payload required reaction wheels to provide attitude control during payload operation because torque coils would have caused too much interference.

After considering the operations of the satellite during different mission phases, it was determined that reaction wheels were necessary during payload operation. Operating the torque coils to maintain pointing during payload operation would have caused interference with the payload, so reaction wheels were required. This led to the selection of the smaller bus architecture.

4.4.2 Mass Budget Analysis with CDR Design Change

Structural analysis was performed for CDR which indicated that the satellite natural frequency was dangerously close to the minimum of 100 Hz required for launch. This analysis is described in Chapter 5. With the knowledge of the mass budget probability distribution, mass was added to stiffen the base plate of the structure, increasing the margin of the satellite fundamental frequency. This explains the shift to the right in the post-CDR curves in Figure 4-2.

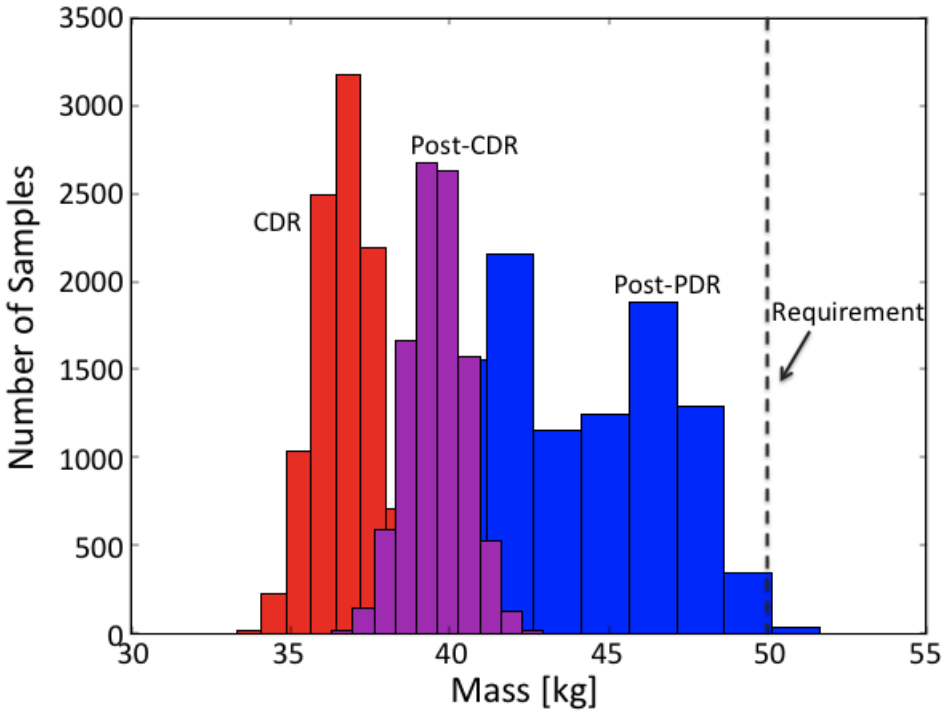

Figure 4-1: Histograms of mass budget Monte Carlo analysis over the course of the program

4.4.3 Results of Mass Budget Analysis

The histogram step is shown in Figure 4-1. It is apparent that the post-PDR distribution is significantly more uncertain than the later distribution because the width of the distribution is the widest. The redesign step is also apparent when comparing the CDR and post-CDR design change because the added stiffness increases the mass, shifting the curve to the right.

Figure 4-2 shows the resulting PDFs of the histograms. It is useful to see that there is significant margin on the mass at CDR and post-CDR.

These PDFs allow complexity and standard deviation to be calculated. Both of these quantities decreased as the program progressed, but that in itself is not especially useful. One would expect the uncertainty in the program to decrease as the design is developed. However, these quantities can also be computed by subsystem.

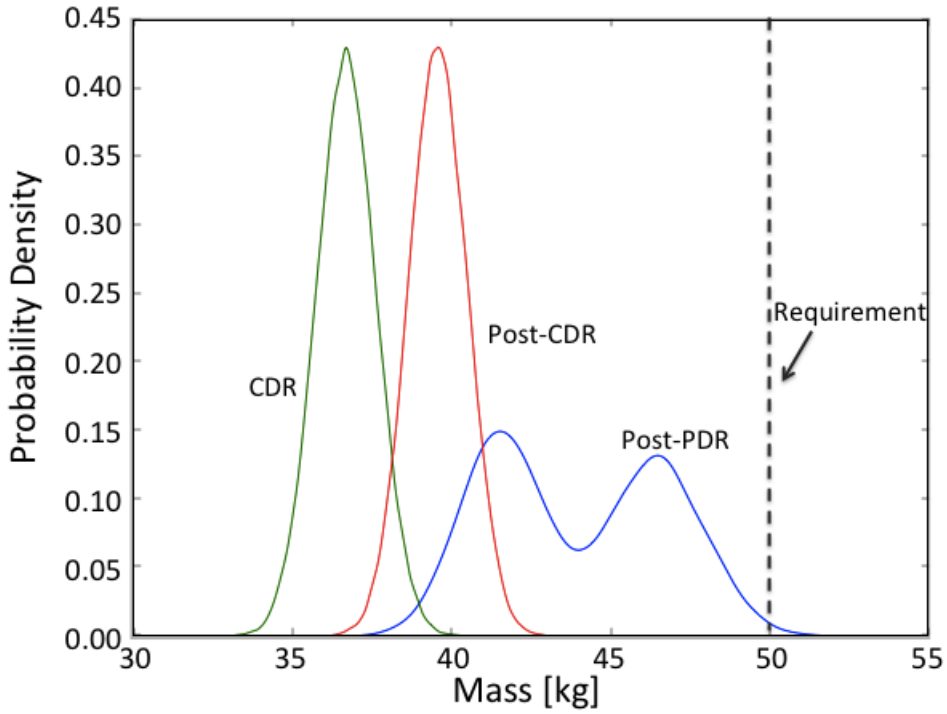

Figure 4-2: Probability Density Functions of mass budget Monte Carlo simulation over the course of the program

The complexity of the post-PDR system mass is 10.6 kg, the complexity of the CDR system mass is 3.9 kg, and the complexity of the post-CDR design change system mass is 3.8 kg.

Table 4.1 gives the complexities of each subsystem over the course of the program. It is important to note that the subsystems are inter-related. For example, in the post-PDR subsystems, the structure had the highest complexity because of trades involving power and ADCS. Still, it is useful to see which subsystems are most affected by design trades.

Additionally, it is clear that the wiring harness became one of the greatest sources of uncertainty after CDR. While the rest of the design had evolved, the wiring harness had barely begun to be conceptualized. This figure highlights the need for the team to incorporate wiring harness into the design as soon as possible. Comparing the

wiring harness complexity with the other subsystem complexities supports the need for extra resources to be spent on developing the wiring harness design.

Table 4.1: Subsystem Mass Complexities after CDR

Subsystem	Complexity [kg]
Payload Antenna System	0.34
Cable Harness	2.3
Solar Panels	1.15
ADCS	0.45
Thermal and Structures	1.93
Battery Box	0.96
Avionics Box	1.32
VLF Receiver Box	0.40
VLF Transmitter Box	1.043

4.5 Mass Budget Analysis Conclusion

This analysis shows that it is possible to use the existing mass budget tracking infrastructure combined with the latest statistics on sources of uncertainties in mass budgets to characterize the uncertainty in space system designs. Additionally, the analysis showed that there was significant margin on the mass even when accounting for the full span of the subsystem mass uncertainties based on historical data. Finally, this analysis showed the relative complexity of the different subsystem masses and helps to highlight where to best focus resources over the course of the program.

Chapter 5

Finite Element Analysis

Uncertainty analysis and sensitivity analysis can also be incorporated into other system models. For structures, the structural finite element model is the primary subsystem model. The purpose of finite element models of structural dynamics is to ensure that spacecraft can survive launch. Launch can be simulated through testing on a vibration table and in a shock simulator setup, but this testing is expensive to repeat if structures fail. Accurate finite element modeling can help reduce program testing costs.

Finite element modeling is a method of finding approximate solutions to structural problems. Structures are discretized into elements called a mesh so that the structure can be represented by a system of equations. Typically software programs such as the NASA Structural Analysis (Nastran) software are used to assist in finite element analysis. Computer-Aided Design (CAD) files can be imported into Patran (the Nastran front-end model building tool) and then a mesh of the structure is built.

One of the most important quantities of interest of spacecraft structural analysis is the natural frequency of the spacecraft, and this is heavily influenced by the mass of the system. The natural frequency of spacecraft need to be above the frequency of launch load inputs to avoid excessive stresses from excitations of the resonances of the structure. Small spacecraft in particular are held to a high natural frequency requirement because small spacecraft are often secondary payloads on launch vehicles carrying very expensive large spacecraft. Failure of a small spacecraft would not only

impact the small spacecraft but could potentially damage the primary spacecraft on the launch vehicle. Thus it is important to all stakeholders of a launch vehicle that spacecraft maintain high resonant frequencies.

With the uncertainty in the mass budget characterized in Chapter 4, we can determine the effects of mass budget uncertainty on the spacecraft natural frequency. In this chapter, we present an analysis of the effects of the TERSat Mass Budget uncertainty on the spacecraft finite element analysis.

5.1 Literature on Spacecraft Structure Uncertainty

Recent work in uncertainty of spacecraft structural analysis uses Monte Carlo and Sensitivity Analysis of complex finite element analysis to characterize system uncertainty. Uncertainty of dynamic structural response has been treated in two ways: either by characterizing the uncertainty or designing the interfacing systems to be robust to this uncertainty.

Earlier work dealt with uncertainty of simpler structural models. Uebelhart (2006) presented analysis of simplified telescope spacecraft finite element models [37]. These models were generated for a range of designs in the design space and each model was evaluated for structural performance and robustness to uncertainty. In this case, structural performance was defined as pointing accuracy and performance analysis consisted of frequency response analysis with inputs from control systems such as jitter.

When structural dynamics have large uncertainties, engineers can accomodate the unknown spacecraft response with control systems. With the Middeck Active Control Experiment (MACE) program, How and Miller (1994) developed control systems for MACE to demonstrate active control of a space structure accommodating large uncertainties in the structural model [19]. Uebelhart, Cohan, and Miller (2006) explored a similar issue with designing a combined optomechanical-control system for the Modular Optical Space Telescope (MOST) program [36].

To characterize effects of input uncertainties in spacecraft structural models, Schuëller (2007 and 2009) built a model of the International Gamma Ray Astrophysics Laboratory (INTEGRAL) spacecraft and described Monte Carlo and gradient-based sensitivity analysis of this model [27] [28]. However, he did not describe in detail the basis for the input uncertainties for mass. We can extend Schuëller's technique by defining mass input uncertainties for analysis of the uncertainties in outputs of spacecraft structural models.

5.2 TERSat Structural Design

The TERSat structural design is illustrated in Figure 5-1. The structure consists of five isogrid plates and one flat plate. The subsystem components are contained in aluminum chassis. All components are alodined to prevent oxidation. External components are secured to the structure with interface brackets. The TERSat structure interfaces with the launch vehicle through a ring on the base of the structure.

5.3 Finite Element Analysis Baseline

This section describes the TERSat structural analysis of launch loading of the pre-build finite element model. It includes analysis approach, inputs, assumptions, and results. The TERSat PQR model has positive margins of safety (MOS) on all components and meets the 100 Hz natural frequency requirement. The stress margins were computed for a +/- 20G load input in each axis with a Factor of Safety for Yield Stress (FS_y) of 2 and a Factor of Safety for Ultimate Stress FS_u of 2.6 per the UNP Stress Analysis guidelines.

Finite element analysis considered the +/- 20G load conditions per the UNP guidelines. However, the model was set up such that random vibration inputs could be analyzed in preparation for future testing and model validation.

This analysis was built in MSC/Patran and run using Nastran.

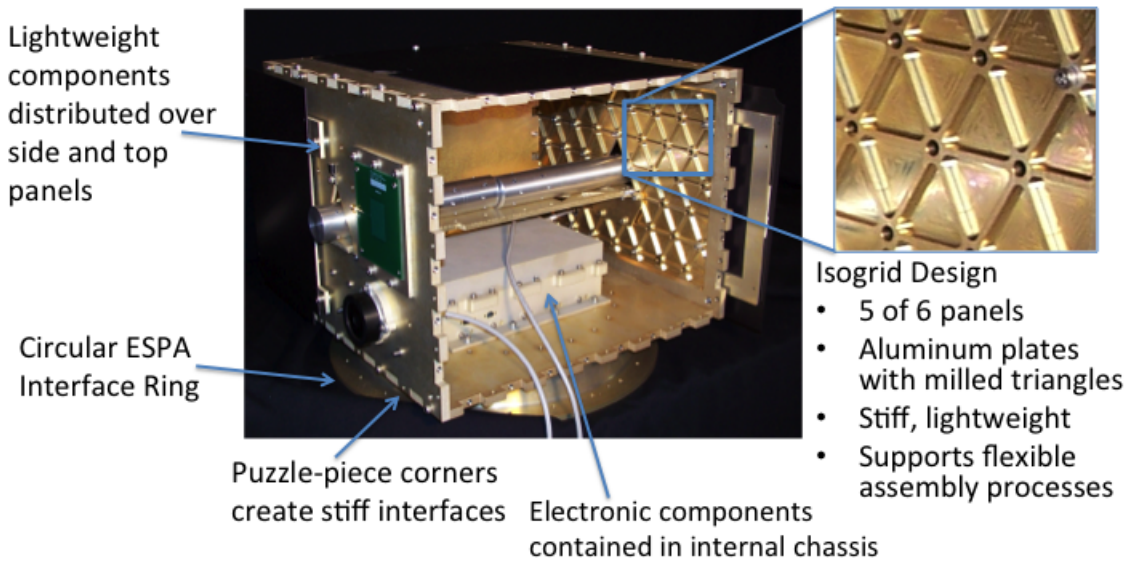

Figure 5-1: TERSat Structural Design Summary

5.3.1 Inputs

Materials

A summary of the materials used is in Table 5.1.

Table 5.1: Materials Data

	Al6061-T6	A286
Use	Isogrid panels, Chassis	Fasteners
Source	MIL-HDBK-5	MIL-HDBK-5
Modulus (psi)	10e+06	2.91e+07
Density ($\frac{lb}{in^3}$)	0.0975	0.287
Poisson's Ratio	0.33	0.31
Sy (psi)	3.6e+04	1.2e+05
Su (psi)	4.2e+04	1.6e+05

Margin of Safety Calculation

Factors of Safety were taken from the UNP Stress Analysis guidelines and were defined as follows:

- $FS_y = 2.0$
- $FS_u = 2.6$

Margin of Safety was calculated using the equation:

$$MOS = \frac{AllowableLoad}{DesignLoad \times FS} - 1 \tag{5.1}$$

Thus, a positive margin of safety indicates acceptable stress levels.

5.3.2 Assumptions

The TERSat finite element model uses the assumption that non-structural elements will not add any stiffness, which adds to the conservatism of the launch loading model. Non-structural elements were modeled as additional mass with no stiffness by adjusting the appropriate bus panel densities. However, some elements such as

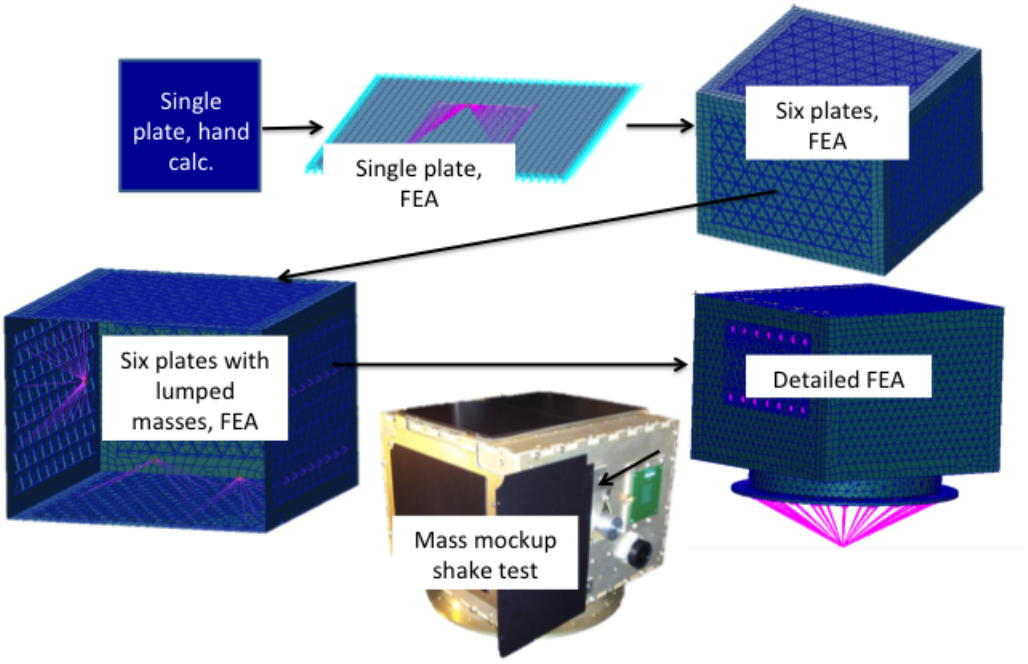

Figure 5-2: Finite Element Analysis Approach

the solar panels, while not designed for the purpose of adding to the stiffness of the structure, would incidentally increase the overall stiffness. The mechanical fidelity of non-structural components has not been fully developed and thus only the additional mass was accounted for.

5.3.3 Model Approach

The TERSat modeling approach is described in Figure 5-2. The current state of the modeling is a detailed FEA model with all structural elements and hand calculations for fastener and pressure analyses. Modeling began with hand calculations using plate theory and the NASA isogrid handbook, and then progressed through increasingly detailed models to the current version.

Boundary Conditions

The model was fixed in space using a standard setup for Random Vibration analysis. An RBE2 element connected the lightband interface mounting locations to a point in space and then the point in space was fixed in translation and rotation.

Finite Element Analysis Description

The model was loaded with +/- 20 Gs in each direction by scaling 1G results. This input is understood to be a conservative bounding of launch loading per the UNP stress analysis guide. There are no prominent buckling modes anticipated in this system so the results are symmetric.

Thermoelastic analysis was not run on the FEM because all of the structural elements are made of Al-6061 T6 and therefore have the same CTE, so the results would be 0 stress for all nodes for any temperature variation. However, some of the non-structural components such as the solar panels and PCBs have a much lower CTE than aluminum. For example, the CTE of a PCB is about 17 ppm/C and the CTE of pure polyimide is about 12 ppm/C versus the 23 ppm/C of aluminum (material information from Matweb.com). Therefore when nonstructural elements are modeled the thermoelastic analysis will be a key loading condition for localized stress conditions.

Finite Element Modeling Description

The TERSat finite element model is shown in Figure 5-3. Initially, the bus panels were modeled as shell elements using the material and topological properties recommended in the NASA isogrid handbook. However, some checks of modal analysis of flat plates using this setup compared with results using detailed meshes of the isogrid including ribs found significant differences, so the more detailed mesh was used.

The bus is modeled using a combination of shell elements for the isogrid skin and beam elements for the isogrid ribs. The isogrid nodes are equivalenced so that the beam elements and shell elements transfer forces properly to each other. The rim

of the isogrid was modeled by quadrilateral (quad) shell elements, with equivalence nodes to mate with the isogrid boundaries. The lightband adapter ring was also modeled as tetrahedral elements.

Component boxes are modeled as tetrahedral (tet) elements. The density of these component boxes was adjusted to account for the masses of the component contents, such as parts, connectors, and wiring. To estimate this density, the conservative density of water rule of thumb was applied. The mass of each component box was calculated by measuring the overall volume envelope of each box and multiplying it by the density of water. The density of each box was then adjusted to meet this mass. The masses were checked against the mass budget prediction to ensure it exceeded the items called out in the budget.

Connections between components were made using RBE2 elements. This connection type did not allow for good bolt force calculations in the FEM, but the future work section will address this point. Fastener analysis information came from using extremely conservative loading information and using hand calculations to estimate bolt stress. The RBE2 elements used the nodes around the top of each through hole as dependent nodes and a node on the mounting surface as the independent node.

5.3.4 Baseline Analysis Results

Analysis of Baseline CDR Design

The modal analysis results of the baseline TERSat CDR FEA are shown in Table 5.4. This analysis indicates that the TERSat system will meet the 100 Hz requirement. However, the system first mode is highly sensitive to the mass distribution in the spacecraft. A margined mass total was assumed for this analysis and some non-structural mass was accounted for far from the mounting location to exaggerate the cantilever effect.

A screenshot of the eigenmode is shown in Figure 5-4 illustrates the rocking motion of the lowest structural mode.

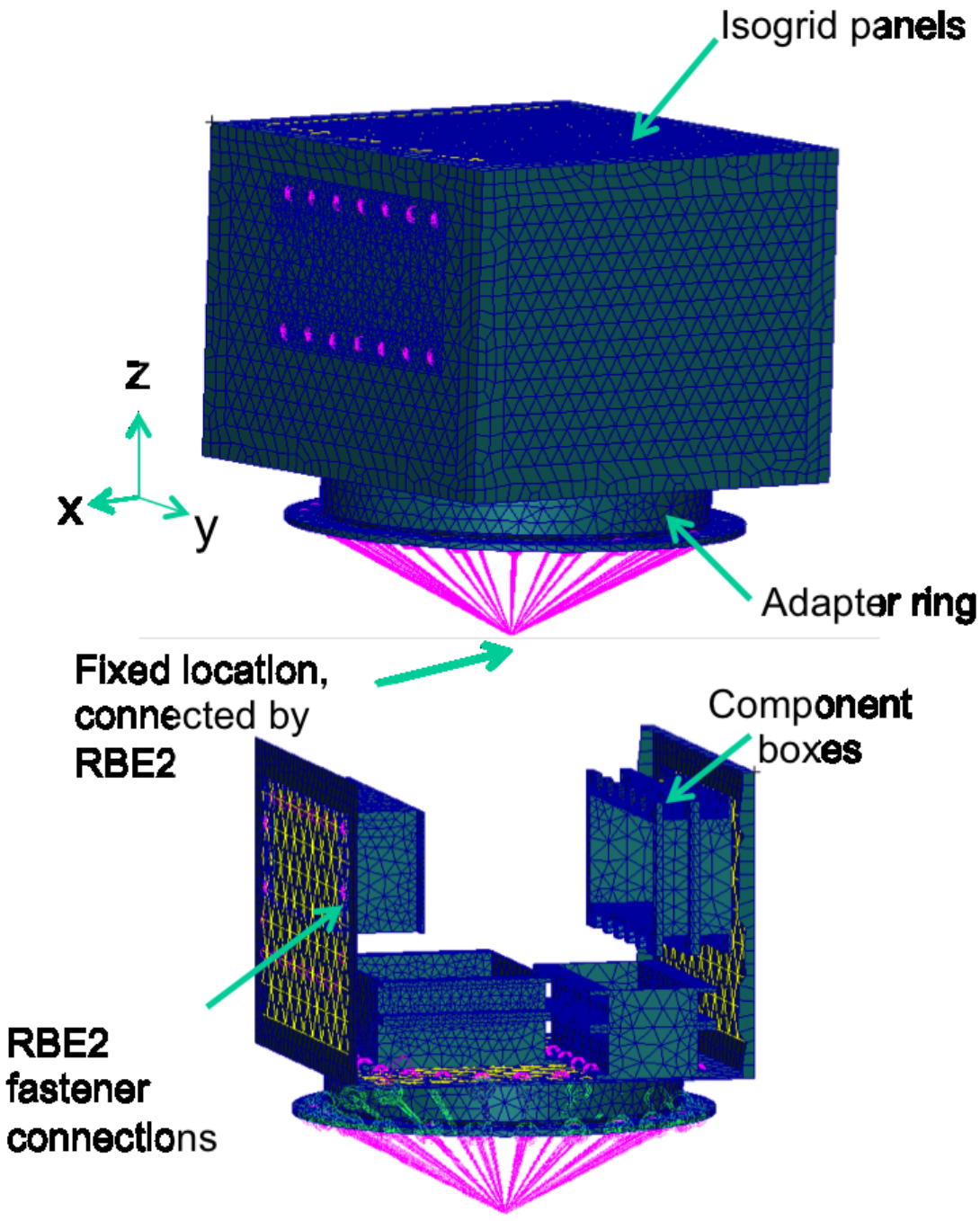

Figure 5-3: Finite Element Analysis model summary

Table 5.2: Modal Analysis Results, First Iteration

Mode number	CDR Frequency [Hz]	Description
1	101	Full spacecraft rocking
2	112	Side panel drum mode with rocking motion
3	172	top panel drum mode
4	204	HPE box mode
5	220	Avionics box mode

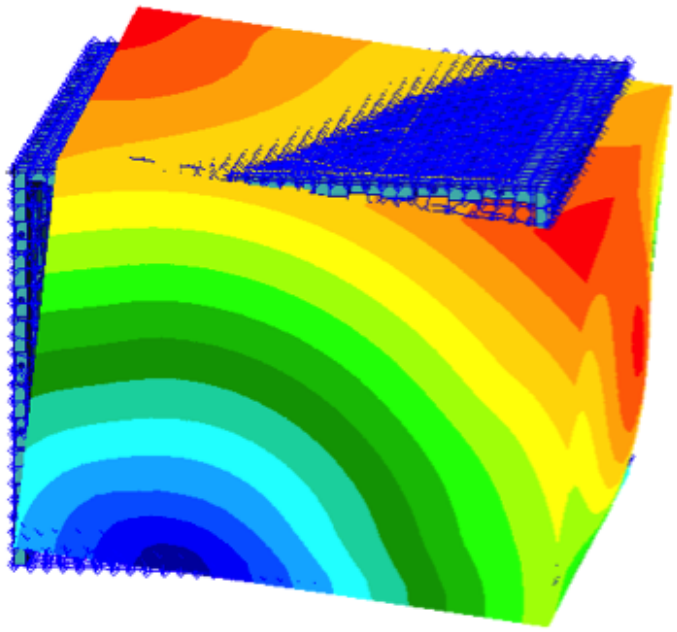

Figure 5-4: First mode of 101 Hz

A summary of the stress analysis results is shown in Table 5.3. All components have positive margins of safety and most components have large positive MOS. The two highest stress results are bolded for emphasis. All primary structural elements (spacecraft bus panels and the lightband adapter ring) had positive margins of safety. The highest stress occurred in the z panel isogrid plate that interfaces with the adapter ring and is illustrated in Figure 5-5.

The lowest stress was on a battery box mounting tab. This stress appears to be generated by a torqueing of the battery box under load due to asymmetric mounting locations. A minor modification of the battery box is under consideration to add additional mounting tabs for thermal reasons, and this modification would greatly

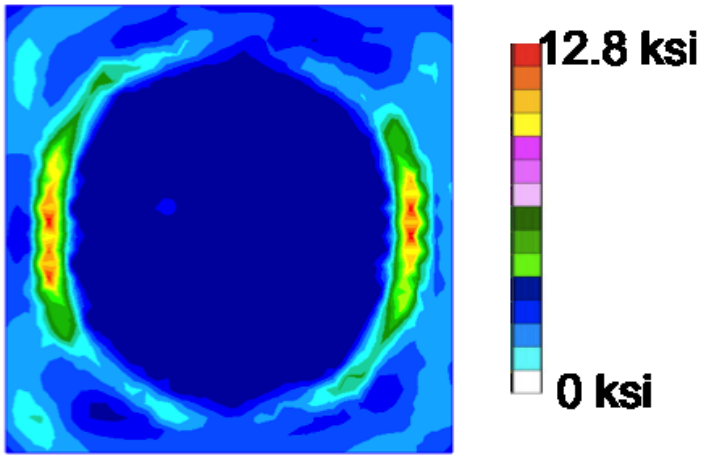

Figure 5-5: Stress analysis results of ESPA interface spacecraft panel

reduce the stress in the battery box. Additionally, the stress is concentrated in just two nodes at a mounting location, where an RBE2 connects these nodes to the isogrid panel. A more complicated analysis would account for the diameter of the bolt head in the RBE2 node selection, and this would eliminate the nonphysical stress concentration to give more accurate results.

Table 5.3: Stress Analysis Results, First Iteration

Components	X [ksi]	Y [ksi]	Z [ksi]	MOSy	MOSu
Panels					
ESPA Panel	12.8	5.7	7.6	0.4	0.26
Side Panels	4.7	1.9	1.9	2.81	2.42
Top Panel	0.6	0.4	0.7	24.94	22.28
Component Boxes					
Battery Box	10.5	8.1	13.3	0.34	0.21
VLF Receiver Box	11.4	12.2	7.7	0.48	0.33
HPE Box	9.0	7.6	7.6	0.99	0.79
Avionics Box	11.4	4.5	5.7	0.58	0.41
Additional Structural Members					
ESPA Interface Ring	11.4	7.6	7.9	0.58	0.42

Analysis of Revised Design

Monte Carlo analysis of the CDR-level structural model (described in more detail in Section 5.5 indicated a 21 % chance of failing the 100 Hz requirement. This

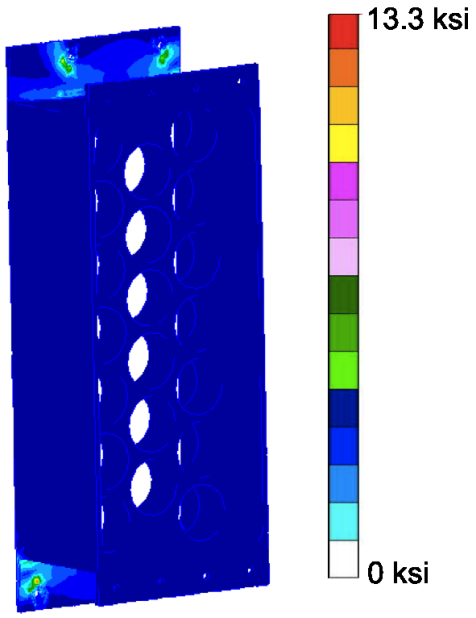

Figure 5-6: Stress analysis results of the battery box

precipitated a design change. Because of the significant mass margin we were able to switch the base plate to a flat plate design rather than an isogrid design, essentially trading risk of resonant frequency requirement failure for risk of mass requirement failure. As the latter was low, this was an acceptable trade.

Because of the large margin available in the mass budget, the bottom isogrid panel was changed to a flat plate. This increased the margin from 1 Hz to 16 Hz on the first mode.

Table 5.4: Modal Analysis Results, First Iteration

Mode number	Frequency [Hz]
1	116
2	126
3	166
4	194
5	222

An updated model based on the new, post-CDR layout was analyzed for PQR. The updated modes are listed in Table 5.5. While the base panel was changed to improve the stiffness of the model, the new component box placement also reduced

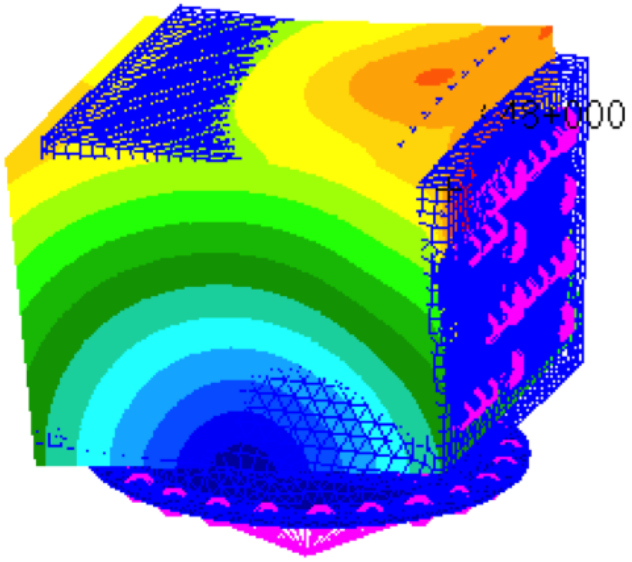

Figure 5-7: Revised first mode of 109 Hz

the stiffness. This is because there were fewer component boxes in the corners of the base panel, which had previously increased the stiffness of the structure. If the mode drops, this layout can be tweaked but would allow less room for wiring.

Table 5.5: Modal Analysis Results, First Iteration

Mode number	Frequency [Hz]
1	109
2	120
3	164
4	203
5	227

The first mode is a rocking motion, as illustrated in Figure 5-7.

Due to time constraints, the static analysis load case set was reduced to a single load case of 20 Gs applied in all three axes simultaneously. The resulting maximum stresses were 12 ksi in the component boxes (with the maximum stress at the battery box mounting interface) and 6.2 ksi in the panels (at the interface with the ESPA ring). This gives a positive minimum MOS of 0.2 ksi. As the analysis is highly

conservative due to the combined load case and yields very satisfactory results, no further analysis was done.

5.3.5 Baseline Analysis Summary

In section, we summarize the results of the TERSat PQR structural analysis. The conservative analysis indicates positive margins of safety on all components for the UNP input loading guidelines and that the design meets the 100 Hz requirement. Additional model fidelity improvement steps are noted for future work.

Three key areas remain for future work: nonstructural element analysis, bolted joint analysis, and random vibration analysis for model correlation.

The nonstructural element analysis will involve building finite element models of the nonstructural elements and incorporating those into the FEA. For example, as the flight PCB design is developed, it will be added to the Avionics box and then checked for stresses, natural frequency, and thermoelastic stresses. Solar panels will be added to the side panels as shell elements. These advances will be important for checking for thermoelastic stresses and tracking the mass distribution for modal analysis reasons.

Second, the bolted joints connected the component boxes to the bus will be modeled in greater detail. Cbush elements will placed in each mounting location and connected to the mounting holes using RBE3s with the node selection determined by bolt head diameter. Further, the elements around mounting locations will be checked for acute geometries leading to high stresses, and remeshed if needed. These steps will improve the accuracy of the battery box mounting MOS.

Finally, a random vibration analysis will be run on the structure in preparation for shake testing. The output of this analysis will be a set of acceleration curves at key locations on TERSat showing the response in G2/Hz over a range of frequencies. This will be overlayed with the responses measured by accelerometers. This overlay will not only serve as a check on the natural frequency highlighted by the sine sweep test, but it will also give a better understanding of the damping in the system and if there are resonances or coupling at higher frequencies.

5.4 Mass Budget Uncertainty Inputs

After a detailed model has been developed, input uncertainties can be propagated. To determine the effects of mass budget uncertainty on the natural frequency of the spacecraft, we must translate the uncertainties of the mass budget into uncertainties in the finite element model inputs.

Table 5.6 shows the composition of the different structural areas with margin for each component based on the AIAA mass growth allowance, as detailed in Chapter 4, for the PQR Monte Carlo structural analysis.

Table 5.6: Density Inputs to Finite Element Analysis

Group	Mean Density $[\frac{lb}{in^3}]$	Density Standard Deviation $[\frac{lb}{in^3}]$
X Panels	0.19	0.016
Y Panels	0.18	0.013
Payload box	0.38	0.028
Bus Electronics Box	0.38	0.035
Battery Box	0.58	0.044

Thus, there are eight densities that will be varied in this analysis. For this analysis, we assume these parameters are independent. In future work it will be important to consider how the dependence of these variables.

5.5 Monte Carlo Analysis of the TERSat CDR Structural Model

The Monte Carlo analysis sampled values of the eight subsystem densities using a gaussian distribution per Section 5.4. For each set of densities, the baseline input file was copied and updated to these densities. Then a bash file was used to run the analysis files. A Python script drew the values of the analysis output frequencies and generated a histogram.

This histogram was then turned into a PDF using Kernel Density Estimation (KDE). This KDE analysis used gaussian distributions because this is the default in

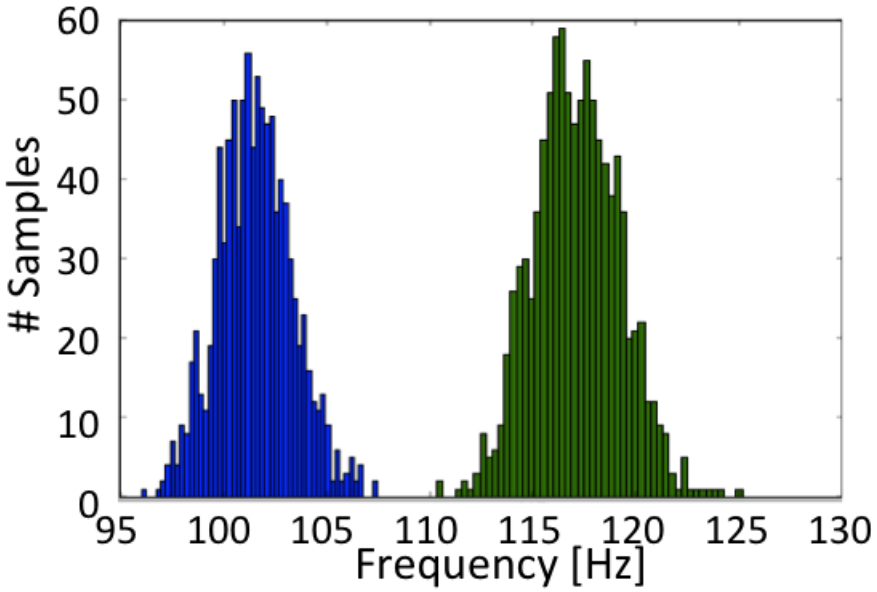

Figure 5-8: Histogram of Monte Carlo Analysis Results of CDR versus post-CDR

the Python Numpy library. However, the literature indicates that the shape of the input distributions do not have a significant effect on the results. The bandwidth of the distributions was determined using Scott's Rule.

A histogram and probability density function of the CDR and post-CDR design change are shown in Figures 5-8 and 5-9 respectively.

Analysis of the two PDFs gave an exponential entropy complexity value of 7.7 Hz for the pre-redesign case and 8.89 Hz for the post-redesign case. This is because the post-redesign case was heavier and mass uncertainty is proportional to the mass of the subsystem (with the aforementioned correcting factors for type of subsystem and subsystem maturity). For this case, the complexity is not as useful a metric for comparison of the two values than the probability of failing the requirement.

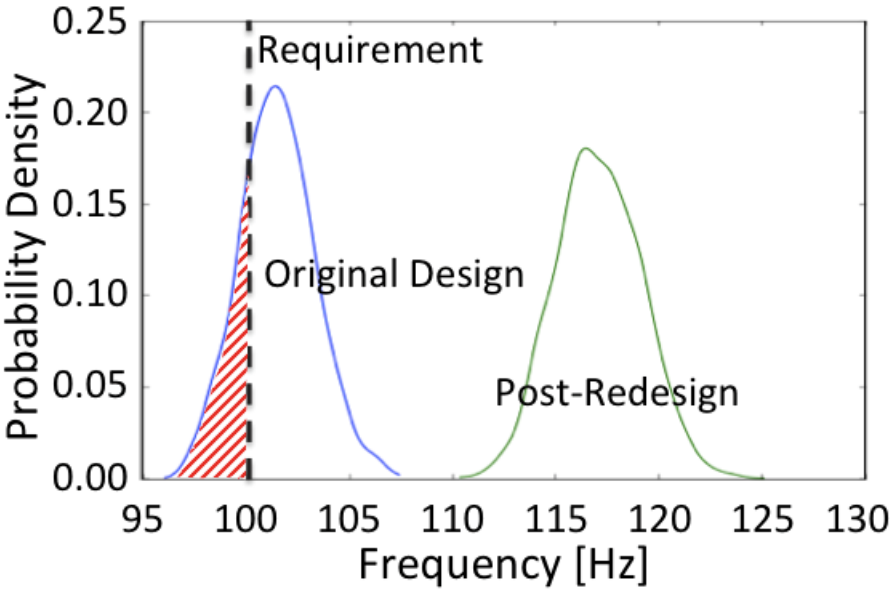

Figure 5-9: Probability Density Function of Monte Carlo analysis results of CDR versus post-CDR

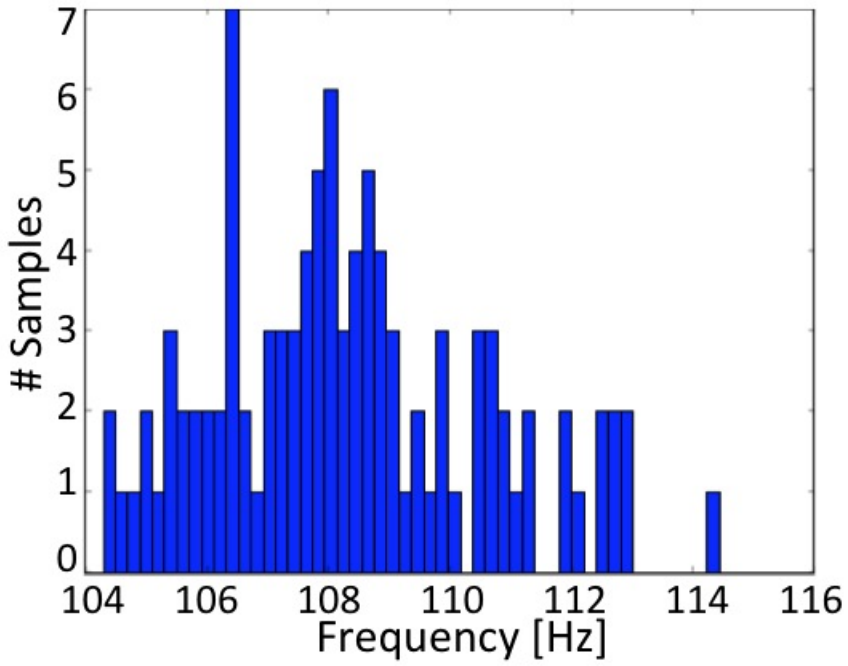

Figure 5-10: Histogram of Monte Carlo Analysis Results

5.6 Monte Carlo Analysis of TERSat PQR Structural Model

The same process was used to analyze the TERSat PQR model. Figure 5-10 shows a histogram of the results of this analysis and Figure 5-11 shows the resulting probability density function.

This PDF indicates that the probability of failing the 100 Hz requirement is less than 1%.

5.7 Sensitivity Analysis of TERSat Structural Model

Schuëller (2007 and 2010) [27] [28] illustrated gradient-based sensitivity analysis of a spacecraft structure finite element model. We apply a simplified version of this

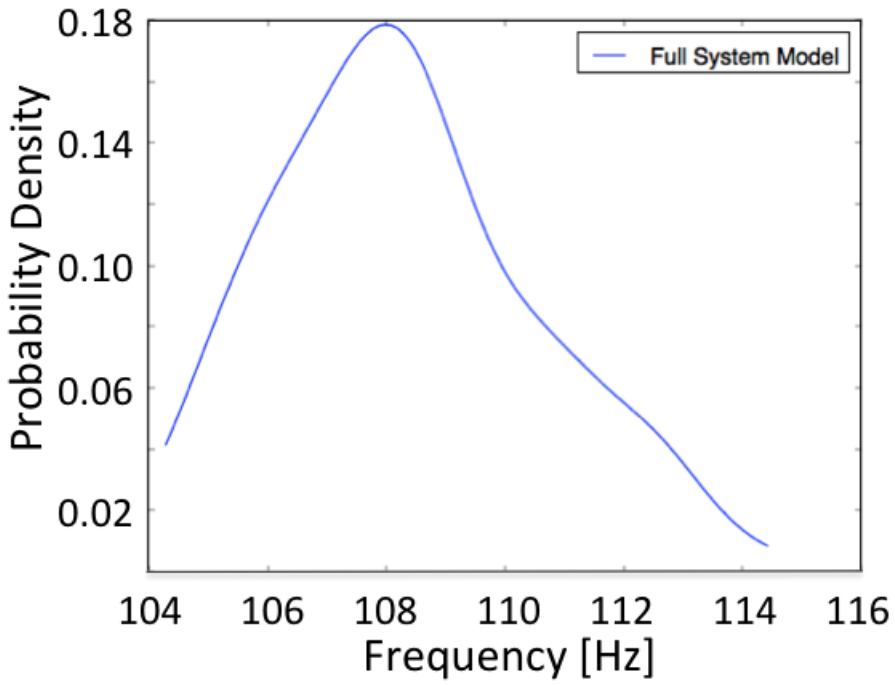

Figure 5-11: Probability Density Function of Monte Carlo analysis results

technique to the TERSat structural model. While in Schueller's work, he is trying to identify the ranked N most important contributors to model uncertainty out of a much larger number of contributors, in this section we are only trying to rank a small number of contributors to uncertainty. The steps of this analysis are as follows:

1. Determine the nominal value of the input parameters
2. Compute a set of N_0 samples with direct Monte Carlo sampling with reduced standard deviation for input parameters
3. For each sample k of the N_0 samples, evaluate $r(x_k)$ and difference from nominal response (r_0)
4. Calculate partial derivative with finite differences
5. Evaluate relative importance with Equation 5.4

Next each of these was sampled 5 times. For each run, all inputs were held constant except for the variable under test. b_k is also used for correlation with the sample input and response. Figure 5-12 shows the relation of the input densities versus the resulting frequencies.

Note that on this scale the results appear to be linear. Best fit lines for each set of points result in a R^2 value of 0.99 or better. From these best fit lines we can use the slope as an estimate of the partial derivative of the nominal results with respect to each input value. The partial derivative can also be found using finite differences. The deviation from the nominal response can be calculated according to $b_k = r(x_k) - r_0$. This can then used find the partial derivative using Equation 5.2.

$$\frac{\partial r}{\partial x_j} = \frac{b_k}{\delta x_j} \tag{5.2}$$

Next, each partial derivative is scaled by the standard deviation of the input uncertainty for the larger model as shown in Equation 5.3. This allows us to consider both the impact of input uncertainties and their scales.

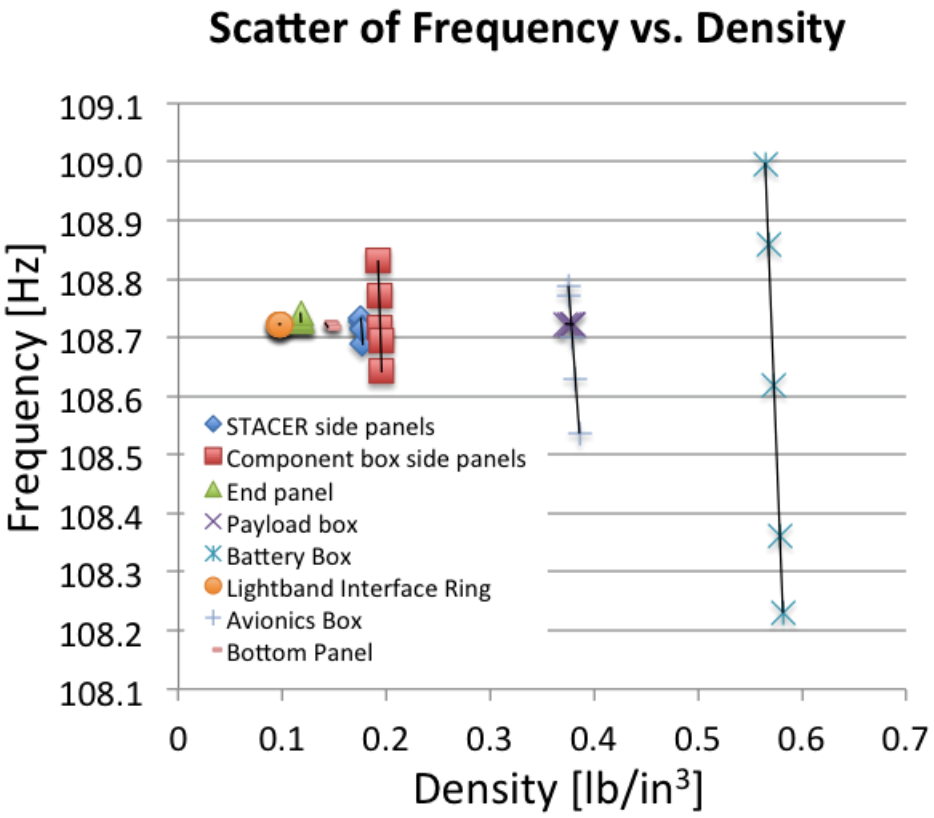

Figure 5-12: Probability Density Function of Monte Carlo analysis results

$$I = \frac{\partial r}{\partial x_j}\sigma \tag{5.3}$$

Note that this results in a measure of importance with units of frequency [Hz]. While in this example unscaled results would have the same units, it is also possible to do this analysis with parameters in addition to mass. Using this equation allows future work to use consistent units.

Finally, this measure of importance is compared with the standard deviation of the full system model output, which in this case is 2.21 Hz according to Equation 5.4.

$$RelativeI = \frac{I}{\sigma_{full}} \tag{5.4}$$

Table 5.7 shows the results of this analysis.

Table 5.7: Sensitivity Analysis Results

Rank	Relative Importance	Group
1	89%	Battery Box
2	40%	X Panels
3	38%	Bus Electronics Box
4	14%	Y Panels
5	9%	+Z Panel
6	1%	-Z Panel
7	0.1%	Payload Box
8	$1\times10^{-}11$	LIghtband Interface Ring

These results show that the most influential mass uncertainty is the battery box. This makes intuitive sense; the battery box has a high inertial relative to the center of rotation (as discovered in the preliminary modal analysis). It also has a high uncertainty relative to the rest of the system.This indicates that the subsequent change to the mass of the battery box should have an effect on system frequency. Similarly, the masses of the isogrid panels and the avionics box should also have an effect.

The mass of the lightband adaptor ring has no effect on the natural frequency of the system. This is unsurprising because the lightband adaptor ring is so stiff that it easily supports its own mass and will not flex at the resonance of the rest of the

system. For similar reasons, the mass of the flat panel attached to the adaptor ring will have relatively low impact.

One interesting result of this study is that the mass of the payload box has little effect on the natural frequency of the spacecraft. Historically, instruments are one of the most uncertain subsystems. By placing the payload box at the base of the structure and centered, this design turns out to be robust to changes in payload mass. This was not intentional in the design, but these results yield a useful lesson learned: When possible, use boundary conditions to design advantage by placing components with high mass uncertainty in locations where they are likely not to influence the structural modes. Future work could further explore placement of uncertain components to ensure minimal effect of uncertainty of a particularly uncertain subsystem.

5.8 Conclusion of Finite Element Analysis Uncertainty Propagation

In conclusion, we have demonstrated that it is possible to characterize the effects of mass budget uncertainty on spacecraft structural response to reduce risk. We demonstrated the use of uncertainties in mass budgets as inputs in structural finite element analysis. We demonstrated Monte Carlo and gradient-based sensitivity analysis.

Chapter 6

Lessons from the TERSat Prototype

While predictions of input uncertainties are useful to the development process, it is important to assess whether the subsystem designs predicted to be most uncertain in this methodology were actually the most altered in the build of the actual prototype. The TERSat prototype was built in the fall of 2012, and some changes were made to simplify assembly with the very small team available for this effort. Many smaller, non-structural changes were made and the masses changed significantly in the battery box, the payload antenna, and the wiring harness. By coincidence these changes balanced each other in overall system mass.

The primary changes from the PQR design are described in this chapter. Then the effects of these changes on the mass budget and structural analysis are discussed.

6.1 Changes to the outside of the TERSat design

Figure 6-1 shows the outside of the TERSat prototype. It also shows added brackets and hardware that was not identified prior to the PQR design; while it was known that small components would require brackets they had not been designed.

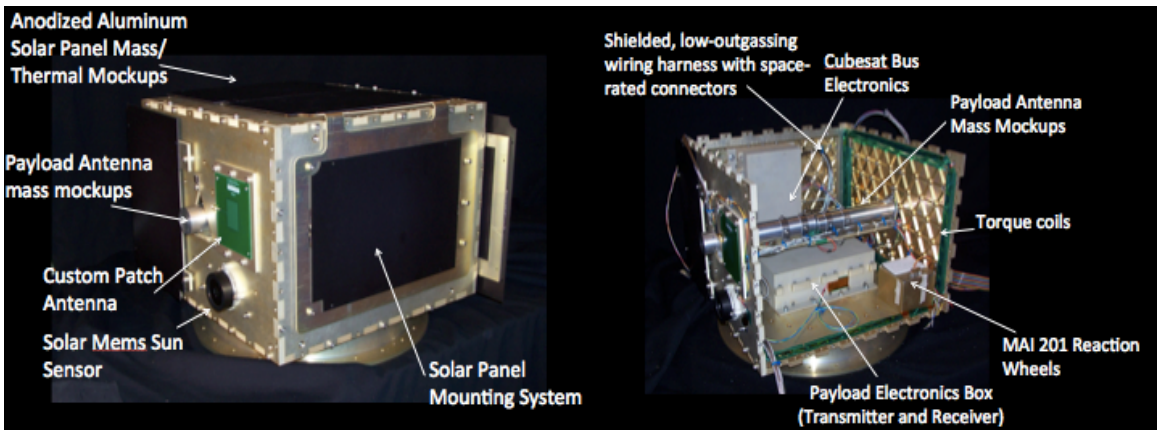

Figure 6-1: Photographs of the TERSat Prototype show the addition of smaller components

6.1.1 Solar Panels

Prior to PQR, TERSat was designed to use the solar panels from a previous MIT satellite program which used scrap cells from Loral Space Systems hand-soldered and assembled by students. This design was undesirable because of the low quality and reliability of the assembled solar panel as well as the labor required for manufacture, but this was the only option prior to PQR due to cost. However, around the time of PQR the Vanguard solar panel company was looking for a small satellite partner to fly some flight-qualified solar panels which were left over from another (cancelled) space program. These panels happened to meet the TERSat power, mechanical, and electrical requirements and this partnership allowed the TERSat team to improve the projected performance of the solar panels. However, these panels required additional bracketing because they were not custom-built for TERSat. This bracketing added mass. Luckily, the solar panels were higher efficiency than the original design, so less area was required and the mass of the new panels plus the additional bracketing was similar to the original design, with the added benefit of additional stiffness from the new brackets.

6.1.2 Development of Miscellaneous Brackets for Non-structural Elements

Small external items did not have mounting fixturing designed prior to the start of fabrication due to time constraints, and these brackets were filled in as needed. These items were the communications antennas and the sun sensors. Because there was not enough time to analyze these components, the mounting brackets were over-designed to ensure sufficient stiffness for launch loads. These were inefficient for mass, but because the mass budget uncertainty analysis indicated large margins, this was not a cause for concern. In contrast, schedule was a major concern and having characterized the uncertainty in system mass thoroughly allowed this valuable flexibility late in the development process.

6.2 Changes to the inside of the TERSat design

The internal changes consisted mainly of three items: the addition of a "bridge" between two structural panels to support the payload STACER antenna, reduced battery mass, and development of the cable harness.

6.2.1 STACER Mounting Bridge

The difficulty of mounting the STACER antenna was underestimated prior to final detailed design and fabrication. The original concept assumed a much lower mass and a smaller volume of the antenna, meaning that each antenna could be supported by a small bracket to the nearest wall. However, it turned out that the antenna in its housing was larger than could be supported by this design.

6.2.2 Power Distribution System Design

The power system was originally designed for a 1 kW payload transmitter. However, around CDR the payload analysis indicated that only 32 W would be used during payload operation. Because there was already a CDR-level design that met mass

requirements, the batteries were not scaled down accordingly by PQR. However, after further discussion with the power distribution system manufacturer (Clyde Space) it was determined that switching to a standard ClydeSpace battery technology (lithium polymer batteries) from the TERSat CDR design (NiCd batteries) would greatly simplify the work required for ClydeSpace, reducing the NRE. Thus, the battery mass was reduced to meet only the 32W payload needs and the battery chemistry was changed to lithium polymer. This greatly reduced the mass of the battery system.

6.2.3 Cable Harness Development

The cable harness went through several iterations before the final version. This was due in part to the high mass uncertainty revealed in the mass budget uncertainty analysis. These many iterations allowed an efficient design to be incorporated as the spacecraft assembly was planned out.

6.3 Modification of the Payload Antenna after Testing

The payload antenna underwent a design change after vibration testing identified a design issue. This testing was useful in identifying and fixing a design problem early enough that large changes were not necessary later in the build process. This testing was a perfect example of the power of the "unk-unk," or unknown unknowns, that cannot be revealed through modeling alone. It illustrated why the philosophy of "test early and often" can never be fully replaced by pure-modeling approaches to structural design.

6.3.1 Unit Under Test

The unit under test was the engineering development version of the TERSat STACER antenna in its housing in the stowed configuration, which is consistent with the spacecraft launch configuration. This fixture was secured to the interface plate using two

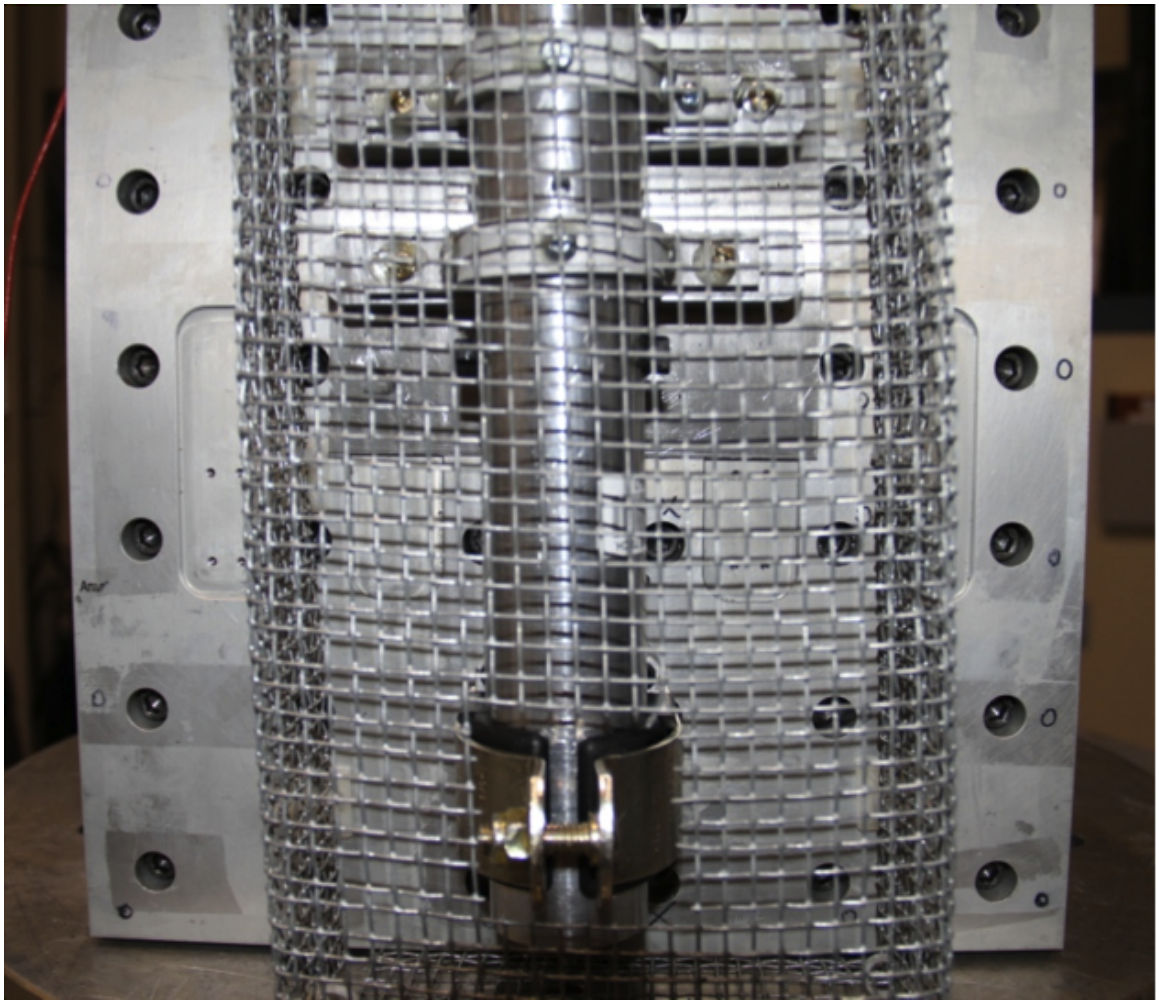

Figure 6-2: TERSat STACER Shake Test Unit. The STACER was secured to the shake test interface plate with clamps to simulate the mounting of the STACER to the TERSat structure. A mesh cover protected surrounding workers from accidental deployment of the STACER.

flight-like brackets and one clamp in place of a bracket. The clamp was necessary because the housing was based on an earlier design that did not allow for brackets to be bolted into the housing in that location.

The STACER antenna is a long piece of beryllium copper sheet metal wound into a cylinder. The inside of this winding is secured to a rod running through the center of the antenna, and the outside is secured to the housing. Figure 6-2 shows the unit under test.

Because of previous experience with student shake tests, initially a mesh cover

enclosed the test setup to prevent any injury from loose hardware. Happily, this mesh cover proved to be unnecessary for this particular test and was removed for convenience for later axes.

6.3.2 Test Setup

The test covered sine and random vibration testing. The UNP specification lacked a standard for shock so shock was not done in this testing. Sine and random vibration testing were both performed in each axis prior to proceeding to the next axis.

6.3.3 Test Anomalies

While the inside and outside of the antenna winding were both secured for vibration, the middle windings were not secured. In deployment testing, it had been found that friction was so large it could sometimes prevent consistent deployment even with manual assistance, so it was thought the setup would be sufficiently secured for launch. However, this was not the case.

As shown in Figure 6-3, the middle windings began to shake loose during random vibration testing when the antenna was in the vertical configuration.

6.3.4 Anomaly Resolution

A small piece of sheet metal was cut and a hole was drilled and tapped in the center. This was threaded onto the center rod, acting as a stopper for the windings. This stopper was used for the duration of the testing, and the test was completed successfully. After testing, the STACER deployed correctly. The stopper is shown in Figure 6-4.

6.3.5 Comments and Test Summary

In summary, vibration testing of the TERSat STACER antenna revealed that the middle of the coil could shake loose during vibration testing. A stopper was added at

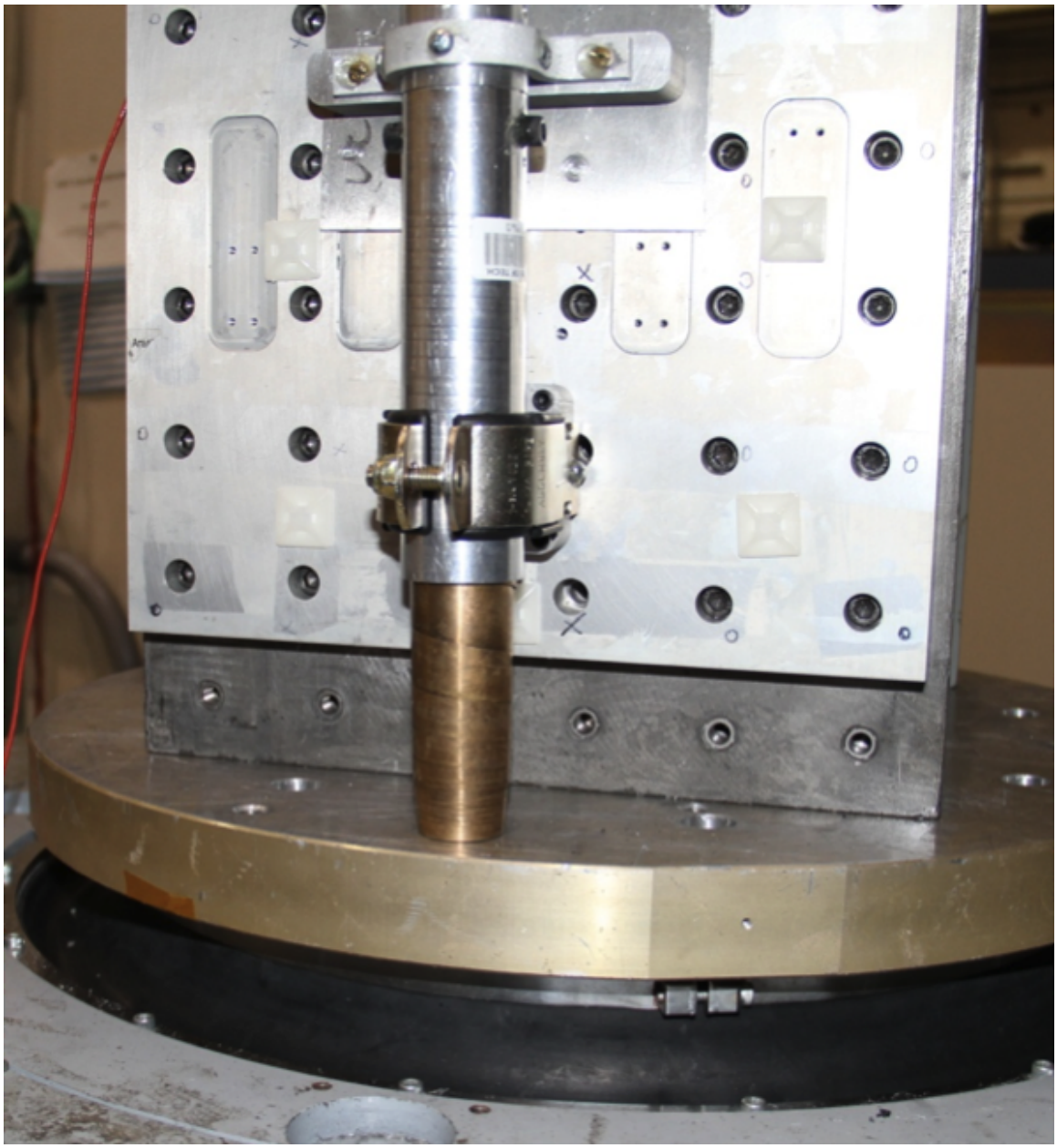

Figure 6-3: TERSat STACER Shake Test Anomaly. The STACER antenna was not adequately secured with the TERSat housing design and shook loose during testing along the axis of the antenna.

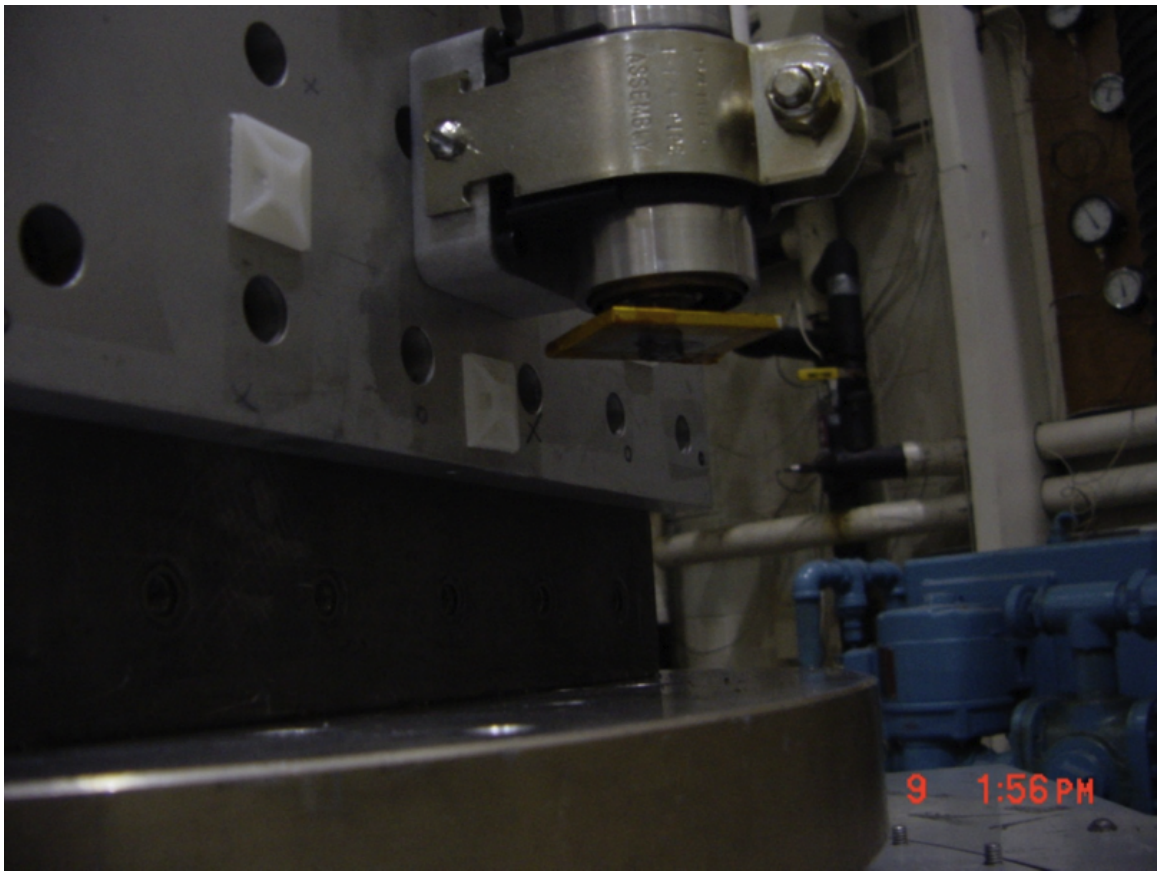

Figure 6-4: The addition of a stopper to the TERSat STACER test setup prevented the STACER from shaking loose during testing along the axis of the antenna.

the end of the internal rod to prevent the coils from moving. This stopper was added early enough in the development of TERSat that no antenna tuning had yet taken place, so there was no difficulty in adding a small component at this early date. A photograph of the STACER after vibration testing is shown in Figure 6-5.

It is interesting to note that had the testing been conducted as part of the full spacecraft testing the anomaly might not have been uncovered. Horizontal testing might not reveal this anomaly because the windings did not have the force of gravity to encourage them to remain slightly farther extended on each vibration cycle. Full spacecraft testing would have been conducted on the horizontal shake table due to size constraints, so shaking along the axis of the antenna might not have revealed this issue.

6.4 Summary of Subsystem Design Mass Changes after As-built Prototype

The as-built masses of two subsystems in the prototype came in significantly under the post-CDR predicted values: the cable harness and the battery box. The battery box mass decreased because models of payload performance indicated that a large battery bank was not necessary, and switching to a smaller COTS battery system would be less complicated to implement. The wiring mass was only a third the original estimate, but was the second-largest mass change in the prototype build. This is because the complexity metric identified wiring as a large source of uncertainty, so the team put great effort into reducing uncertainty in this subsystem. Several iterations of wiring harness prototypes allowed the team to reduce uncertainty, but in doing so also allowed the team to plan out an efficient design and routing prior to integration. Because the margin on the wiring was larger for other subsystems, relying on margin alone may not have had the same results.

While the changes to the subsystems caused mass changes on the order of two kilograms, the changes balanced each other out to keep the system current best

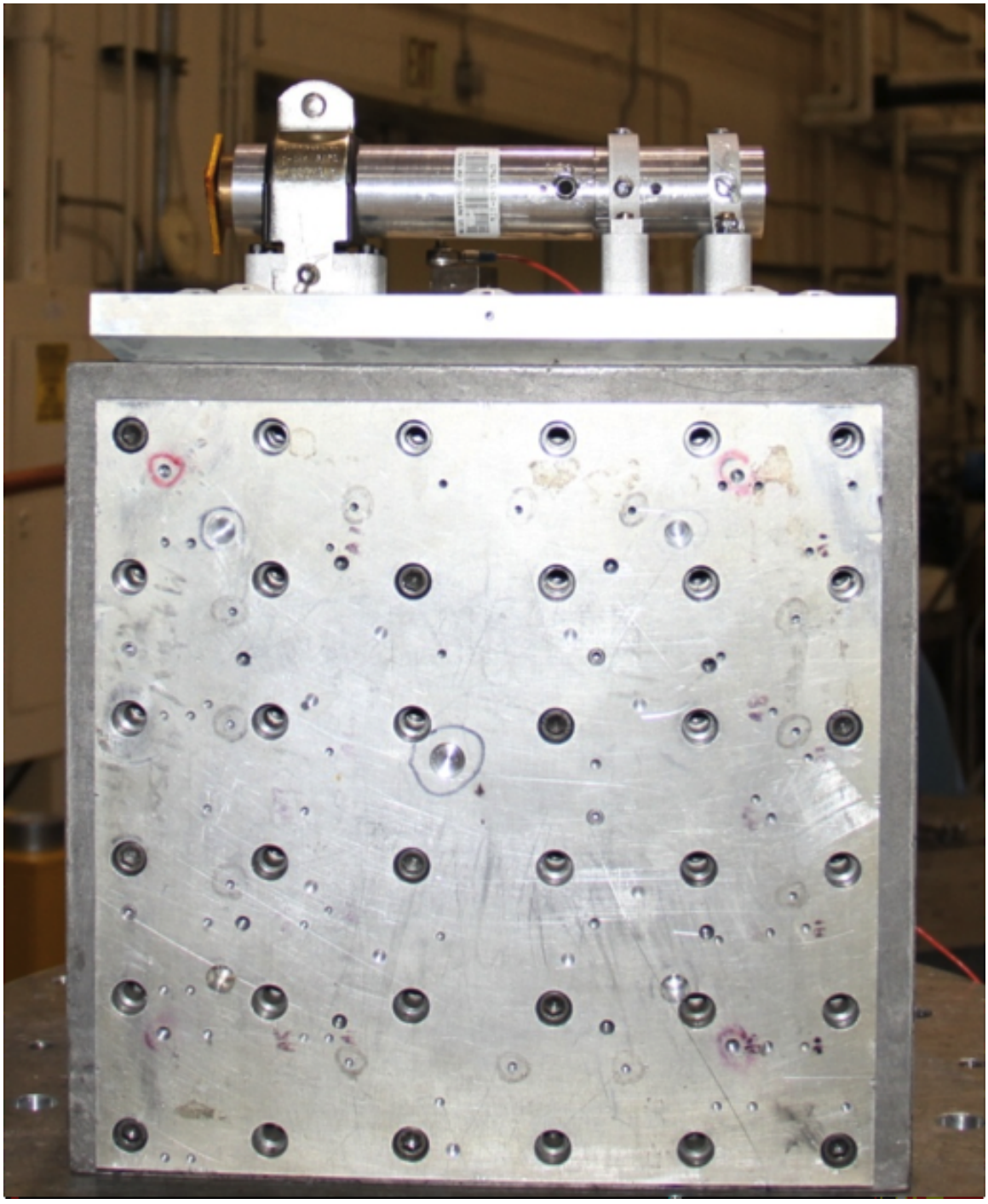

Figure 6-5: TERSat STACER Shake Test, Final Configuration. The STACER assembly successfully completed the rest of the shake test.

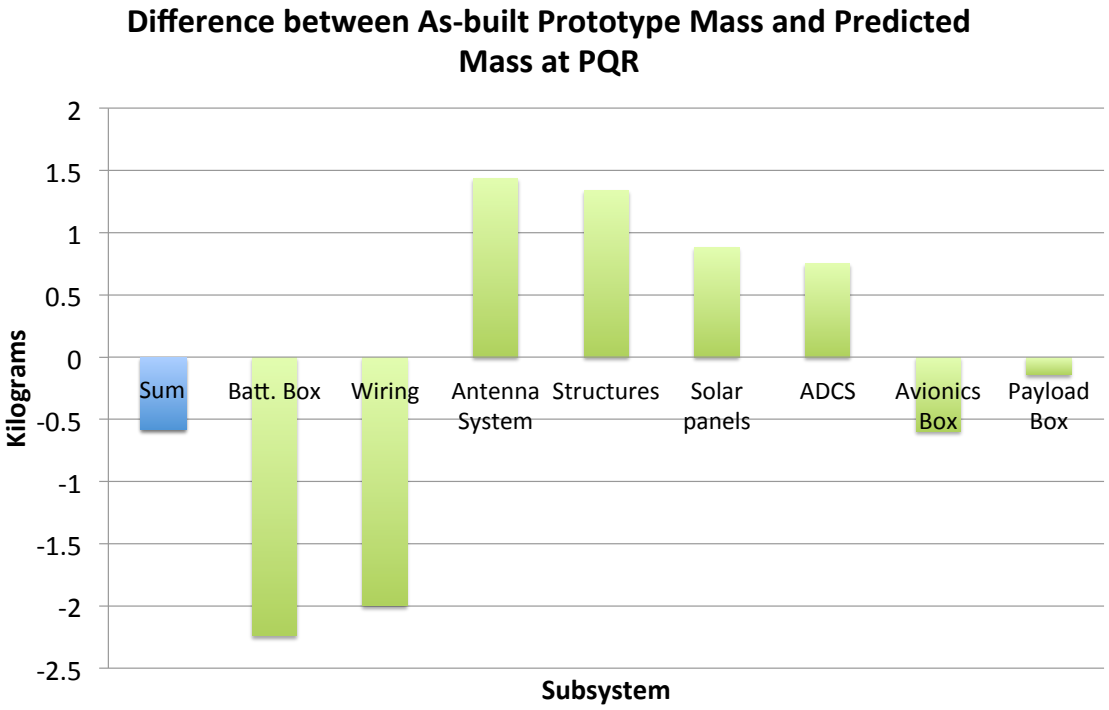

Figure 6-6: Comparison between TERSat subsystem mass predictions at PQR and measured values of the as-built prototype. While there were substantial changes in subsystem masses, the sum of the changes was small (less than 2% of the CBE at PQR

estimate relatively constant.

6.5 Conclusion

In summary, there were many changes to the TERSat design as the prototype was fabricated and assembled. Some of these changes were for technical reasons, such as adding the bridge for the payload antenna mounting. Some were programmatic, such as switching to donated space-rated solar panels and making inefficient mounting brackets to save analysis time.

Comparing these with what was predicted in the earlier chapters of this thesis is difficult because of a chicken-and-egg problem: the outputs of uncertainty analysis were used in the development of the program, so additional resources were allocated to burning down uncertainty.

Chapter 7

Conclusion and Future Work

In this thesis, we have presented a method of characterizing uncertainties in space system design and propagating these uncertainties to determine the effects on quantities of interest in space systems using Monte Carlo and sensitivity analysis to reduce program risk. The Trapped Energetic Radiation Satellite (TERSat) structural design was used as a test case for this analysis. The methodology highlighted the need for a change in the TERSat structure, helping to precipitate the change from an isogrid to a flat plate. Additionally, sensitivity analysis helps to guide placement of the non-structural elements of the TERSat design. Therefore, the methodology helped TERSat to avoid costly redesign and was successful for this test case. However, the methodology has room for improvement in the input uncertainty characterization. Future work should also validate this methodology with additional quantities of interest and additional programs.

7.1 Future Work in Input Uncertainty Characterization

Future work could study additional types of input quantities. While mass inputs are an appropriate first input uncertainty test case, structural models have many inputs to be studied. As demonstrated by Schuëller, material properties such as

Young's modulus or poisson's ratio and properties of composite layups could also be studied using probabilistic techniques. Such uncertainty characterization could be incorporated into the proposed design methodology.

Additionally, future work could investigate how to model interdependencies between subsystems and how this would affect the complexity and Monte Carlo analysis. While TERSat's modular design allowed an assumption of independent random variables, this is not the case for many programs. This could include a study of how to use Design Structure Matrices or N^2 diagrams as inputs to the analysis as these model subsystem interdependencies.

7.2 Future Work in Studying Additional Quantities of Interest

Future work in this area could extend to additional quantities of interest. Within structural analysis, the estimated stresses under random vibration analysis, static, and shock could be analyzed probabilistically. Additionally, other program measures such as schedule could be analyzed with this framework, using historical data of schedule slips of previous program to model input uncertainties.

7.3 Future Work in Validating Methodology with Additional Programs

This methodology should be extended to future programs. While the TERSat test case was successful, the methodology was improved during the course of the TERSat program. Additionally, as a student program the uncertainties in the TERSat development are likely to stem more from inexperience of the engineers than the uncertainties in other programs. By testing the methodology on programs from industry, further areas for improvement could be identified.

7.4 Summary

This work applied uncertainty characterization techniques at different stages of actual spacecraft development to characterize the sensitivity of spacecraft mass budget uncertainty in structural analysis with the goal of more efficiently reducing risk.

The measures of success we defined for this methodology were:

- Quantitative: Demonstrate reduction in risk of failing a requirement
- Qualitative: Guide for layout fine-tuning, improved understanding of uncertainties

For the TERSat test case, the methodology identifies the design issue that the pre-CDR structural design had a 21% probability of failing the natural frequency requirement due to mass increases and verifies that the revised design had a less than 1% probability of failing the natural frequency requirement. Sensitivity analysis of the PQR model shows that placement of the non-structural elements should avoid the battery box.

Bibliography

[1] Aiaa standard mass properties control for space systems (s-120-2006), 2006.

[2] E.F. Arthur. A theory of system complexity. *International Journal of General System*, 1(1):19–33, 1974.

[3] Kenneth L Atkins, Bredt D Martin, Joseph M Vellinga, and Rick A Price. Stardust: implementing a new manage-to-budget paradigm. *Acta Astronautica*, 52(2):87–97, 2003.

[4] David A Bearden. A complexity-based risk assessment of low-cost planetary missions: when is a mission too fast and too cheap? *Acta Astronautica*, 52(2):371–379, 2003.

[5] Eileen A Bjorkman, Shahram Sarkani, and Thomas A Mazzuchi. Using model-based systems engineering as a framework for improving test and evaluation activities. *Systems Engineering*, 2012.

[6] Jacob Bortnik, Umran S Inan, and Timothy F Bell. L dependence of energetic electron precipitation driven by magnetospherically reflecting whistler waves. *Journal of geophysical research*, 107(A8):1150, 2002.

[7] T.R. Browning. Sources of schedule risk in complex system development. *Systems Engineering*, 2(3):129–142, 1999.

[8] Paul D Collopy. A research agenda for the coming renaissance in systems engineering. *2012 Aerospace Sciences Meeting*, 2012.

[9] David Cornelius, Washito Sasamoto, Kevin Daugherty, and Shaun Deacon. Integrated campaign probabilistic cost, schedule, performance, and value for program office support. In *Aerospace Conference, 2012 IEEE*, pages 1–12. IEEE, 2012.

[10] N. Croisard, M. Vasile, S. Kemble, and G. Radice. Preliminary space mission design under uncertainty. *Acta Astronautica*, 66(5):654–664, 2010.

[11] O. de Weck, G. Bounova, R. Keller, C. Eckert, and P.J. Clarkson. Change propagation analysis in complex technical systems. *Journal of Mechanical Design*, 131:081001–1, 2009.

[12] OL de Weck. A systems approach to mass budget management. *AIAA Annual Report*, 2006.

[13] O.L. de Weck and M.B. Jones. Isoperformance: Analysis and design of complex systems with desired outcomes. *Systems engineering*, 9(1):45–61, 2006.

[14] G.F. Dubos, J.H. Saleh, and R.D. Braun. Technology readiness level, schedule risk and slippage in spacecraft design: Data analysis and modeling. *AIAA SPACE 2007 Conference & Exposition*, 2007.

[15] D.L. Emmons, R.E. Bitten, and C.W. Freaner. Using historical NASA cost and schedule growth to set future program and project reserve guidelines. In *Aerospace Conference, 2007 IEEE*, pages 1–16. IEEE, 2007.

[16] Claude W Freaner, Robert E Bitten, Dave Bearden, and Debra Emmons. An assessment of the inherent optimism in early conceptual designs and its effect on cost and schedule growth. *Presentation to the Planetary Science Subcommittee, NASA Advisory Council*, 2008.

[17] RL Gross. Faster, better, cheaper: Policy, strategic planning, and human resource alignment. Technical report, Report Number IG-01-009, NASA Office Of The Inspector General, 2001.

[18] Robert A Helliwell. *Whistlers and related ionospheric phenomena*, volume 1. Stanford University Press Stanford, 1965.

[19] Jonathan How, R Glaese, S Grocott, and D Miller. Finite element model based robust controllers for the mit middeck active control experiment (mace). In *American Control Conference, 1994*, volume 1, pages 272–277. IEEE, 1994.

[20] G. Karpati, T Hyde, H Peabody, and M Garrison. Resource management and contingencies in aerospace concurrent engineering. *AIAA SPACE 2012 Conference & Exposition*, 2012.

[21] K.A. Kipp, S.C. Ringler, E.L. Chapman, and C.W. Freaner. Impact of instrument schedule growth on mission cost and schedule growth for recent nasa missions. In *Aerospace Conference, 2012 IEEE*, pages 1–13. IEEE, 2012.

[22] A.N. Kolmogorov. Three approaches to the quantitative definition of information. *International Journal of Computer Mathematics*, 2(1-4):157–168, 1968.

[23] Fred Kuo and Steve Wilson. Joint confidence level requirement: Policy and issues nasa/tm-2011-216154. Technical report, NASA, 2011.

[24] Benjamin Mossawir, Ivan R Linscott, Umran S Inan, James L Roeder, Jon V Osborn, Steven C Witczak, Everett E King, and Stephen D LaLumondiere. A tid and see radiation-hardened, wideband, low-noise amplifier. *Nuclear Science, IEEE Transactions on*, 53(6):3439–3448, 2006.

[25] B.T. Murray, A. Pinto, R. Skelding, O. de Weck, H. Zhu, S. Nair, N. Shougarian, K. Sinha, S. Bopardikar, and L. Zeidner. Meta ii complex systems design and analysis (coda). Technical report, DTIC Document, 2011.

[26] Mark Scherbarth, Durand Smith, Aaron Adler, Janet Stuart, and Greg Ginet. Afrl's demonstration and science experiments (dsx) mission. Technical report, DTIC Document, 2009.

[27] Gerhart I Schuëller, Adriano Calvi, Manuel F Pellissetti, Helmut J Pradlwarter, Sebastiaan HJA Fransen, and Andreas Kreis. Uncertainty analysis of a large-scale satellite finite element model. *Journal of Spacecraft and Rockets*, 46(1):191–202, 2009.

[28] GI Schuëller. On the treatment of uncertainties in structural mechanics and analysis. *Computers & structures*, 85(5):235–243, 2007.

[29] David W Scott. Feasibility of multivariate density estimates. *Biometrika*, 78(1):197–205, 1991.

[30] Cosma Rohilla Shalizi. Methods and techniques of complex systems science: An overview. In *Complex systems science in biomedicine*, pages 33–114. Springer, 2006.

[31] Cosma Rohilla Shalizi. Complexity measures, 2012.

[32] M.R. Silver and O.L. de Weck. Time-expanded decision networks: A framework for designing evolvable complex systems. *Systems Engineering*, 10(2):167–188, 2007.

[33] George Ralph Sondecker IV. *Identification and evolution of quantities of interest for a stochastic process view of complex space system development.* PhD thesis, Massachusetts Institute of Technology, 2011.

[34] MJ Starks, RA Quinn, GP Ginet, JM Albert, GS Sales, BW Reinisch, and P Song. Illumination of the plasmasphere by terrestrial very low frequency transmitters: Model validation. *Journal of Geophysical Research*, 113(A9):A09320, 2008.

[35] Robert W Thompson, Alan W Wilhite, David Reeves, Douglas O Stanley, and John Wagner. Mass growth in space vehicle and exploration architecture development. *Acta Astronautica*, 66(7):1220–1236, 2010.

[36] Scott A Uebelhart, Lucy E Cohan, and David W Miller. Design exploration for a modular optical space telescope architecture using parameterized integrated models. In *Proc. 47th AIAA/ASME/ASCE/AHS/ASC Structures, Structural Dynamics, and Materials Conference. AIAA*, 2006.

[37] Scott Alan Uebelhart. *Non-deterministic design and analysis of parameterized optical structures during conceptual design*. PhD thesis, Massachusetts Institute of Technology, 2006.

[38] Julie Wertz and David Miller. Expected productivity-based risk analysis in conceptual design. *Acta Astronautica*, 59(1):420–429, 2006.

[39] K. Willcox, D. Allaire, J. Deyst, C. He, and G. Sondecker. Stochastic process decision methods for complex-cyber-physical systems. Technical report, DTIC Document, 2011.

[40] Walter Zucchini. Applied smoothing techniques. Technical report, 2003.